**Atmospheric
Chemistry
and Physics
Discussions**

Observations of NO$_x$, ΣPNs, ΣANs, and HNO$_3$ at a rural site in the California Sierra Nevada Mountains: summertime diurnal cycles

D. A. Day[1,*]**, D. K. Farmer**[1,**]**, A. H. Goldstein**[2]**, P. J. Wooldridge**[1]**, C. Minejima**[1]**, and R. C. Cohen**[1,3]

[1]Department of Chemistry, University of California, Berkeley, CA, USA
[2]Department of Environmental Science, Policy and Management, University of California, Berkeley, CA, USA
[3]Department of Earth and Planetary Science, University of California, Berkeley, CA, USA
[*]now at: Scripps Institution of Oceanography, Univ. of California, San Diego, La Jolla, USA
[**]now at: Cooperative Institute for Research in Environmental Science (CIRES), University of Colorado, Boulder, CO, USA

Correspondence to: R. C. Cohen (rccohen@berkeley.edu)

Title Page

Abstract	Introduction
Conclusions	References
Tables	Figures

|◄ | ►|

◄ | ►

Back | Close

Full Screen / Esc

Printer-friendly Version

Interactive Discussion

Abstract

Observations of NO, NO_2, total peroxy nitrates (ΣPNs), total alkyl nitrates (ΣANs), HNO_3, CO, O_3, and meteorological parameters were obtained from October 2000 through February 2002 at 1315 m a.s.l., 38.97° N, 120.6° W on Sierra Pacific Indus-
5 tries land, adjacent to the University of California Blodgett Forest Research Station (UC-BFRS). We describe the data set with emphasis on the diurnal cycles during summertime 2001. We show that transport of the Sacramento urban plume is a primary factor responsible for diurnal variation in total reactive nitrogen mixing ratios as well as in NO_x, ΣPNs and ΣANs, all of which exhibit a late afternoon/early evening peak. In
10 contrast, HNO_3 has a peak just after local noon indicating that HNO_3 is in near steady state during the day with production due to photochemistry and removal by deposition and mixing with the background free troposphere. Boundary layer dynamics influence mixing ratios of all species in the early morning. Analysis of the morning feature suggests that higher mixing ratios of NO_x and HNO_3 persist in the residual layer than in
15 the nocturnal boundary layer indicating the presence of nocturnal sinks of both species. Nighttime observations also indicate large HNO_3 and ΣANs production through oxidation of alkenes by NO_3.

1 Introduction

Tropospheric NO_x ($\equiv NO+NO_2$) radicals exert strong influences over ozone (O_3) and
20 organic aerosol production (e.g. Kroll et al., 2006). Oxidation of NO_x produces peroxy nitrates (RO_2NO_2, PNs), alkyl and multifunctional alkyl nitrates ($RONO_2$, ANs), HONO, NO_3, N_2O_5 and nitric acid (HNO_3), all of which are thought to be removed from the atmosphere more rapidly than NO_x. However, rates of removal vary by at least an order of magnitude (Farmer et al., 2006, and references
25 therein) and in some locations these higher oxides are important sources of NO_x (e.g. Singh et al., 1992; Smyth et al., 1996; Horowitz et al., 2007). Document-

ing and testing our understanding of the mechanisms affecting atmospheric NO_x and NO_y ($NO_y \equiv NO + NO_2 + \Sigma RO_2 NO_2 + \Sigma RONO_2 + HNO_3 + HONO + NO_3 + N_2O_5 + \ldots$) remains a significant challenge, in large part because of the analytical challenge of measuring all of the key components of NO_y is one that is still not adequately met. For example, ANs, especially those derived from isoprene, terpenes, and aromatics, are calculated to be important reservoirs of reactive nitrogen, however, only one group has reported field measurements of specific isoprene-derived nitrates (Grossenbacher et al., 2001; Grossenbacher et al., 2004; Giacopelli et al., 2005) and one group has reported field measurements of aromatic nitrates (e.g., Schneider et al., 1998; Woidich et al., 1999). Laboratory studies of isoprene nitrate formation remain controversial with a range of a factor of 3 in the reported yields (Tuazon and Atkinson, 1990; Chen et al., 1998; Chuong and Stevens, 2002; Sprengnether et al., 2002; Patchen et al., 2007; Paulot et al., 2008).

In our own work, we have reported field observations of the sum of all molecules with the chemical formula $RONO_2$ (ΣANs) and also the sum of all peroxynitrates, molecules of the form RO_2NO_2 (ΣPNs). The ΣAN measurements have been used to conclude that isoprene nitrate yields are at the low end of the range of reported laboratory measurements (Horowitz et al., 2007). Moreover, analysis of these measurements have shown that varying the range of isoprene-nitrate yields (from 4.4% to 12%) results in a constrained range of lifetimes of isoprene nitrates (from 5 h to 1.5 h) within the continental boundary layer (Perring et al., 2008). This analysis also yields coupled values for the recycling efficiency (92% to 74%) at which reaction of isoprene nitrates result in another AN rather than production of NO_x or HNO_3, demonstrating that reaction of isoprene nitrates generally maintains the AN functionality.

Here, we use measurements of the summertime diurnal cycle of NO_y partitioning among the species NO, NO_2, ΣPNs, ΣANs and HNO_3 as constraints to evaluate our understanding of the processes affecting partitioning of NO_y within the continental boundary layer. The measurements were made near the University of California – Blodgett Forest Research Station (UC-BFRS), 5 h downwind of the edge of the Sacramento

Printer-friendly Version

Interactive Discussion

urban sprawl. Previous analyses of nitrogen oxide observations from this site have emphasized the importance of ΣANs and their identity as the "missing NO_y" (Day et al., 2003), day-of-week effects that couple NO_x to OH mixing ratios (with consequent observable effects for reactive VOC) (Murphy et al., 2007), the effects of temperature on summertime NO_y partitioning (Day et al., 2008), and comparison to upwind (Granite Bay) and downwind (Big Hill) observations (Murphy et al., 2006). Observations of fluxes of NO_{yi} have been discussed and analyzed to provide evidence for upward and downward components of vertical exchange indicating that a large source of OH in the forest canopy exists (Farmer and Cohen, 2008). Here, we examine our understanding of the effects of biogenic emissions, chemistry and transport as they impact the diurnal variation in NO_y partitioning and NO_{yi} mixing ratios. We use these diurnal variations to evaluate our understanding of some of the key chemical and dynamical processes involved in determining production and removal rates of various categories of NO_y.

2 Experimental

2.1 Site description

Measurements were made from October 2000 to February 2002 on Sierra Pacific Industries (SPI) land near the University of California – Blodgett Forest Research Station (UC-BFRS) (1315 m a.s.l., 38.9° N, 120.6° W) (Fig. 1). The site is a managed ponderosa pine plantation located in the mid Sierra Nevada Mountains 75 km northeast of Sacramento, CA (pop. 410 000, Greater Sacramento Area $\cong$ 2 million) in a sparsely populated region. The climate at this site is discussed in detail in Dillon et al. (2002) and Kurpius et al. (2002). Briefly, the climate of the western Sierras has a wet and a dry season. The dry season (May–September) is characterized by warmer temperatures, low rainfall, clear skies, and steady, regular east/west, upslope/downslope winds. The wet season (October–April) is characterized by cooler temperatures, moderate rainfall or snowfall, and less regular wind patterns. Temperatures peak in summer (June–

August) and are lowest in late-fall through winter. The annual cycle at UC-BFRS is similar to the climatology in the city of Sacramento reviewed by Dillon et al. (2002) except that it is typically 5–10°C colder at the higher elevation of UC-BFRS. During the dry season, upslope winds of 2–3 m/s from the southwest are observed during the

5 day, switching at 18–19 (local standard time) to downslope winds of 0.5–2 m/s from the northeast with a return to southwesterlies at 7–8. Summer measurements described in this paper span the months of June–September (2001) and are characterized by almost no precipitation (<2 cm total), consistently warm temperatures (average daily peak=24°C), and extremely persistent and regular daily wind flow patterns.

10 A 12 m walk-up tower was used as a sampling platform and supporting equipment was mounted on the tower or housed in a small wooden shed and a modified refrigerated shipping container. The inlet for the TD-LIF instrument described below was located at 11 m above ground level (a.g.l., 9 m before February 2000) and at ~3–5 m above the forest canopy. For most concentration and flux measurements (NO_{yi}, VOC,

15 O_3, CO_2, H_2O, etc.) made prior to 1999, sample air was drawn from ~9 m a.g.l. or 3–6 m above the tree canopy (Lamanna and Goldstein, 1999; Schade et al., 1999a; Goldstein et al., 2000; Goldstein and Schade, 2000; Dillon, 2002; Dreyfus et al., 2002) and then beginning in 1999 from 11–12 m a.g.l. (3–5 m above canopy) (Bauer et al., 2000; Goldstein and Schade, 2000; Kurpius et al., 2002; Kurpius et al., 2003; Spauld-

20 ing et al., 2003). During 2004–2005 eddy covariance flux measurements of NO_{yi} were conducted at 14.3 m a.g.l. (7 m above canopy) (Farmer and Cohen, 2008). The site was powered by a diesel generator located ~130 m to the northwest. During the day, southwesterlies were strong enough that plumes from the generator were rarely observed. At night, the winds were weaker and more variable in direction, and occasional

25 short-duration plumes from the generator were observed.

2.2 TD-LIF measurements

Thermal dissociation – laser induced fluorescence (TD-LIF) was used to measure NO_2, total peroxy nitrates (ΣPNs), total alkyl nitrates (ΣANs), and HNO_3 at UC-BFRS. The

3439

TD-LIF technique is described in detail in Day et al. (2002) and application of the technique to both urban and rural ground sites is described in Day et al. (2003, 2008), Rosen et al. (2004), Cleary et al. (2005, 2007), Murphy et al. (2006) and Farmer et al. (2006, 2008) and the free troposphere in Murphy et al. (2004) and Perring et al. (2008). Briefly, for the UC-BFRS TD-LIF instrument, an ambient sample flows rapidly through an inlet and is immediately split into four channels. The first one is used to observe NO_2; the second is heated to $180°C$ causing thermal dissociation (TD) of ΣPNs, the third to $350°C$ for additional TD of ΣANs, and the fourth to $550°C$ to include TD of HNO_3. The temperatures noted are characteristic of the particular oven design, and are proxies for higher temperatures of the gas flowing within the ovens. The dissociation of all of these species produces NO_2 with unit efficiency. Differences between the NO_2 signals observed simultaneously from channels heated to adjacent temperature set-points are used to derive absolute abundances of each of these four classes. For example, ΣPNs are the difference in NO_2 detected in the $180°C$ and ambient channels. Both the volatile and semi-volatile components of ΣANs and HNO_3 (i.e., NH_4NO_3) are detected (Bertram and Cohen, 2003; Fountoukis et al., 2007). However, there are no NH_3 sources in the vicinity of UC-BFRS. NH_3 measurements made at UC-BFRS during the summer of 2006 were too low for NH_4NO_3 to exist in equilibrium with the gas phase NH_3 and HNO_3 present (Fischer and Littlejohn, 2007). We assume NH_3 changed little over the last decade at this site. Compounds that decompose into NO such as HONO or organic nitrites are not detected in any of the TD-LIF channels but can be measured with detection of NO (Pérez et al., 2007). A comparison of ΣNO_{yi} ($\Sigma NO_{yi} \equiv NO$(measured by chemiluminescence)$+NO_2+\Sigma PNs+\Sigma ANs+HNO_3$) and total NO_y (measured by catalysis – chemiluminescence) shows that these two values are usually comparable (Dillon, 2002; Day et al., 2003) suggesting that nitrites and non-volatile nitrates are minor at this site.

The inlet (from sample entry through complete dissociation) has a 50–100 ms residence time. In order to ensure maximum transmission of HNO_3 and other "sticky" compounds through the inlet (Neuman et al., 1999; Ryerson et al., 1999), a heating

unit (60°C) was fixed to the PFA tubing upstream of the heated quartz ovens. The inlet consisted of four quartz ovens (120 cm long, 6.4 mm o.d., 3.8 mm i.d.) insulated and mounted in steel electrical conduits. Following the quartz ovens, the pressure was reduced 10-fold by a stainless steel pinhole in order to decrease the residence time and minimize secondary chemistry in the transit via the 20 m PFA tubing to the detection cells. The flow rate in each channel was approximately 1500–2000 standard cubic centimeters per minute (sccm). The total flow of approximately 45 l/s at the detection cell pressure of 3 Torr was maintained by the combination of a small roots blower (five-fold boost) and an oil-based mechanical pump (9 l/s).

The TD-LIF instrument is capable of routine, continuous, autonomous, in situ measurements that are accurate (15%) and sensitive. Typical detection limits were 90 ppt/10s (S/N=2) on a background of 1 ppb NO_2 (total dissociated NO_2 in the channel at lower temperature when differencing as in the case of ΣANs and HNO_3) and 30 ppt/10 s on a background of 100 ppt NO_2. The uncertainty in the instrument zero during this experiment was typically ±10 ppt. This uncertainty results from photon counting statistics and from drift in the detection cell laser scatter due primarily to temperature-driven laser alignment changes that occurred rapidly compared to measurement of the instrument zero. In the analysis presented in this paper, 30-min averages were used, reducing the detection limits based solely on counting statistics to 7 ppt and 2 ppt for the above cases. For 30-min data, the detection limits and precision are probably controlled mostly by the zero uncertainty and the relative accuracy of the calibrations.

The instrument was calibrated every 2.5 h using an NO_2 standard (5.85 ppm in N_2, scott specialty gas) diluted to 1–10 ppb in zero air. The calibration mixture was injected (overflow) in the inlet to ensure that the calibration gas mixture passes through a nearly identical flow path to an ambient sample. Zeros were measured approximately every hour, using separate tubing for the pure zero air and the NO_2 calibration mixture to ensure the zero determinations were not compromised by residual NO_2.

We also introduced a variety of diagnostics to check the accuracy of our calibration

and analysis routines. Standard additions of NO_2 were performed 2–3 times per day (through the calibration line). The standard additions were used to confirm that corrections in the calibration due to quenching by ambient water (1–9%) are accurately modeled (Thornton et al., 2000) and to assess the effect of NO_2 on retrieved ΣPNs,
ΣANs, and HNO_3 (Day et al., 2002; Rosen et al., 2002, 2004). Also, every three hours, while continuing to sample ambient air, the temperature set-point of one or more ovens was dropped to the adjacent temperature below the normal sampling temperature in order to confirm that the calibrations of the adjacent cells were precise, relative to one another. This also ensured that measurements of the instrument zero in each channel
were accurate, with no systematic bias between the adjacent channels observed. Approximately twice each week and always after maintenance of an oven, all three ovens were slowly (20°C/min) and simultaneously ramped down from their normal set-points to slightly below the adjacent set-point. This allowed us to determine the temperature at which each class of compounds begins to dissociate and the temperature required
for full dissociation. We never observed a large change in the required set-points and thus kept the set-points constant throughout the experiment.

2.3   Measurements of NO, NO_y, CO, O_3, and Meteorology

NO and NO_y measurements were made at UC-BFRS using NO-O_3 chemiluminescence (Thermo Environmental Co. model 42CTL). A converter of molybdenum oxide (MoO) mesh, maintained at 325°C to convert NO_y species to NO, was located
40 cm downstream from the sample intake. The 30-s measurement cycle was split equally between NO_y, NO, and background measurements. Laboratory experiments conducted following the experiment identified a leak resulting in crosstalk between the NO_y and NO channels. This, in combination with elevated nighttime NO concentrations
(~20 ppt), indicate that the NO measurements may have been affected by a positive bias. Correcting the NO data using results from the laboratory tests and the ambient NO and NO_y observations did not produce convincing results. Therefore, the analysis below uses uncorrected NO data. We estimate that the bias was at most +20–25 ppt.

Printer-friendly Version

Interactive Discussion

Also, where possible, gaps in the NO data set were filled with steady-state estimates from the NO_2 and O_3 measurements combined with the average diurnal cycle of the steady-state term, $NO \cdot O_3/NO_2$. The estimated NO concentrations were used only for calculating ΣNO_{yi} concentrations, and were generally less than 5%.

⁵ Wind speed, wind direction, humidity, temperature, CO_2 and O_3 concentrations, net radiation, photosynthetically-active radiation, and pressure were measured as described in Goldstein et al. (2000) and Bauer et al. (2000). CO measurements were obtained using gas chromatographic separation followed by a reduction gas detector (RGD2, Trace Analytical, Incorporated). The instrument was calibrated using a CO

¹⁰ standard diluted to 50–500 ppb in CO-free zero air. VOC were measured as described in Goldstein et al. (2000), Bauer et al. (2000), and Schade et al. (2001).

2.4 Data processing

TD-LIF data were collected at 1 or 5 Hz and averaged to 10-s means. Nighttime generator spikes produced periods marked by highly elevated (10–200 ppb), variable NO_2

¹⁵ values of short duration (10–500 s), and high $NO_2/\Sigma NO_{yi}$ and $NO/\Sigma NO_{yi}$ ratios. These periods were identified by comparing 10-s NO_2 concentrations to a 20-min running median filter, and all affected TD-LIF (14% nighttime TD-LIF data), NO and CO data were removed prior to averaging and analysis.

Data used in the following analysis are half-hour medians of NO_{yi} and CO data, and

²⁰ means of O_3 and meteorological observations. Table 1 shows the number of 30-min data points available for each compound along with the percent coverage from 1 June through 30 September 2001. In addition, 12 cumulative days in late August and early September (all or parts of 26–31, 19–21 August, and 7–11 September) were removed from the analysis since large effects from forest fires in the region were clearly identified

²⁵ by abnormally high CO and ΣNO_{yi} concentrations.

2.5 Summertime regional transport, emissions and micrometeorology

The role of transport and anthropogenic emissions in the summertime Sacramento plume, as observed at UC-BFRS, are described by Lamanna and Goldstein (1999) and Dillon et al. (2002). Briefly, the upslope/downslope flow pattern that characterizes transport in the western Sierras imposes a regular pattern on concentrations of chemicals that have their source in the Greater Sacramento Area (Murphy et al., 2006). The concentrations of these compounds increase throughout the day during the upslope flow from the southwest (245°). Downslope flow from the northeast (50°) returns cleaner air to the site with minimum concentrations observed in the early morning. Concentrations of long-lived species (e.g. acetylene) typically begin to increase at noon and reach their peak at 22 h (10 p.m. local standard time), 2–3 h after the shift to downslope flow, suggesting that the center of the plume is slightly to the north of UC-BFRS. Concentrations drop gradually after the 22 h peak reaching a minimum in mid-morning (10 h).

The exceptionally regular wind patterns on the western slopes of the Sierra Nevada with strong daytime upslope flow and weaker nighttime downslope flow make the site particularly useful for studying atmospheric chemistry. The upslope flow that brings air from the direction of Sacramento passes across a band of oaks that are strong isoprene emitters downwind of the city. In the morning air from the west with a weak urban influence but strong influence from the oaks arrives first, followed by air that has both strong oak and urban influences. In the evening the downslope return flow brings that same air back over the site along with cleaner air from the high Sierra and free troposphere.

The daily patterns are controlled by solar insolation and temperature cycling, which in turn affect chemistry, biology and meteorology. Surface warming creates a well-mixed boundary layer below the free troposphere. Shortly after sunset, colder surface temperatures drive a much lower stable nocturnal boundary layer underneath a residual layer and the free troposphere. Stable conditions minimize exchange between these

nocturnal layers. In the morning, heating at the surfaces causes this nocturnal bound-
ary layer to break up, mixing down air from the residual layer and forming a convective
mixed layer under the free troposphere.

3   Observations

Figure 2a shows observations (30-min medians) of NO, NO_2, ΣPNs, ΣANs, HNO_3,
$ΣNO_{yi}$, CO, O_3, temperature, and wind direction during a typical summer period (12–
26 July). Skies were clear and no precipitation occurred on these days. The wind
patterns were nearly constant, except during the night of 15 July. Overall, the timing of
variations in CO, O_3, $ΣNO_{yi}$, NO_2, ΣPNs, and ΣANs was similar with peaks late in the
afternoon followed by decreases until early morning. In contrast, NO and HNO_3 peaked
at midday. There is also some variability evident on synoptic time scales. For example,
from 12–16 July, temperature, CO, O_3, $ΣNO_{yi}$, NO_2, ΣPNs, HNO_3, and ΣANs, de-
creased reaching minima on the 15th or 16th. On 17–18 July, temperatures increased,
along with most species. Both the nighttime lows and midday peaks roughly followed
these trends. 21–24 July shows a similar trend when maximum daily temperatures in-
creased steadily from 20 to 29°C. Figure 2b shows an example of relatively uncommon
periods where the winds shifted to the south during nighttime (1, 4 June) and in gen-
eral is a cooler period for summer. Diurnal cycles in the observed mixing ratios are still
apparent although with smaller variation and lower correlation to synoptic variability. In
contrast, Fig. 2c shows a period in mid-September when observed mixing ratios have
stronger diurnal cycles than typical and with stronger correlations to synoptic-timescale
temperature patterns.

Average diurnal patterns of NO_{yi}, CO, O_3, meteorological variables and the NO:NO_2
ratio are shown in Figs. 3 and 4. The points represent median values and the lines
bound the central 68th percentile. Note that NO concentrations shown in Fig. 4 are
the measured NO concentrations, whereas $ΣNO_{yi}$ concentrations in Fig. 3 include both
measured and estimated NO concentrations.

Printer-friendly Version

Interactive Discussion

4 Diurnal patterns of individual reactive nitrogen classes

We observe patterns in the variability of the concentrations on four distinct dynamical timescales: seasonal, synoptic, day-of-week, and diurnal. Seasonal cycles will be the subject of a separate manuscript. Synoptic variability in the summer is, in large part, a temperature effect that is described in Day et al. (2008). Day-of-week patterns and their causes and effects are discussed in Murphy et al. (2006). Here we concentrate on the diurnal variability and restrict our analysis of diurnal patterns to weekday data (Tuesday–Friday). Observations on Saturday, Sunday and Monday display similar patterns in the diurnal cycles of the reactive nitrogen species but at lower overall mixing ratios because of reduced weekend emissions in the region. Also there are some changes in the ratios of species due to NO_x-controlled decreases in OH on weekends.

4.1 ΣNO_{yi}

During summer 2001, ΣNO_{yi} (Fig. 3) peaked during 15–19 h (at 3 ppb) and, coincident with the change in wind flow, decreased gradually to morning lows (1.6 ppb). CO (Fig. 3) peaked about 2 h later, decreased more slowly and reached a broad minimum in mid-morning before rising again. These patterns are largely controlled by transport of the Sacramento plume and its mixing with cleaner air from the high Sierra and free troposphere. Once the urban plume has left the region of strong anthropogenic influence the only additional sources of CO are oxidation of anthropogenic and biogenic VOC and photolytic or temperature-driven emission from plants or soils (Schade and Crutzen, 1999, and references therein; Schade et al., 1999b). Shade et al. (1999b) observed total CO emission rates from a dry grass savanna of $250 \times 10^9\,\mathrm{cm^{-2}\,s^{-1}}$ for typical solar irradiance at UC-BFRS during summer mid-afternoon ($\sim$800 W/m^2). If this surface flux were mixed into an 800 m boundary layer, subject to dilution during the 5-h transect from Sacramento to UC-BFRS (0.31 h^{-1}; Perez and Cohen, 2009), the result would be an additional 1.4 ppb rise observed at UC-BFRS, approximately 7% compared to the observed $\sim$20 ppb rise for 12–17 h.

The additional CO added to the plume through oxidation of biogenic VOC can be estimated using methyl vinyl ketone (MVK) and methacrolein (MACR) observations. In the initial oxidation steps of isoprene, the reactions producing these two compounds also produce the co-product, formaldehyde, at a 1:1 ratio (Fuentes et al., 2000, and references therein). Formaldehyde can be photolyzed or react with OH, always leading to production of one CO molecule (Fried et al., 1997). Observations during summer 2001, on average, displayed a 0.42 ppb increase in [MVK+MACR] from the morning windshift to 17 h. Correcting for chemical loss of [MVK+MACR] due to reaction with OH in the ~2-h transit from the primary isoprene source (for $OH=1\times10^7$ molecules cm^{-3}) yields a total source of 2.4 ppb formaldehyde. The midday lifetime of formaldehyde ($OH=1\times10^7$ molecules cm^{-3}) is approximately 1.5 h (photolysis rate from (UCAR/NCAR/ACD, 2006) H_2CO+OH rate constant from Sander, 2006). Therefore, approximately 75% of the formaldehyde will react, producing ~1.8 ppb CO, or ~9% of the observed CO increase. The isoprene oxidation products and CO will be diluted into different background concentrations as the plume advects from the isoprene source band, however the increases observed at UC-BFRS will be affected proportionally.

Chemical removal of CO is too slow to be important on a 5-h time scale, thus diurnal variation in CO mixing ratios are primarily affected by the intensity of transport of the Sacramento urban plume, the magnitude of VOC oxidation, direct natural emissions and the mixing of the plume into the background atmosphere. NO_y is also affected by these same transport and mixing processes and in addition, natural emissions (from soils) may be a significant source of NO_y, 50–130 ppt or 7–20%, of the 700 ppt midday increase (for surface emission of 5.8–15 ppt NO_x m s^{-1} (Herman et al., 2003; Farmer and Cohen, 2008), 800 m boundary layer height, and dilution at 0.31 h^{-1}; including HNO_3 production and deposition discussed in Sect. 4.3). Unlike CO, NO_y is subject to removal by dry deposition during transport. The occurrence of the peak of ΣNO_{yi} two hours earlier than peak of CO is one indicator that, in addition to the transport, emission and deposition processes are important controls over NO_y.

The diurnal pattern in NO_y at this site is unusual. Urban and rural sites often have diurnal cycles that appear to be primarily controlled by boundary layer height. When the boundary layer is thin, NO_x sources produce nighttime maxima in NO_y and much lower NO_y is observed during the day (Buhr et al., 1990; Parrish et al., 1993; Aneja et al., 1996; Munger et al., 1996; Thornton et al., 2002). Mountaintop sites that are isolated above the boundary layer at night exhibit lower NO_y concentrations at night (Parrish et al., 1993; Zellweger et al., 2000). Although boundary layer height certainly plays an important role affecting the individual classes of NO_{yi} at UC-BFRS, the upslope/downslope flow pattern dominates the diurnal cycle in total NO_y with some modifications to the pattern superimposed through biosphere-atmosphere exchange (Farmer and Cohen, 2008).

4.2 NO_x

The major features in the diurnal cycle of NO, NO_2 and NO_x are:

1) 17–20 h NO_x peak

2) Daytime NO/NO_2 ratio

3) AM peaks

The primary NO_x peak occurred between 17–20 h, later than the 15–19 h peak of ΣNO_{yi} (Fig. 4). The NO_x peak was concurrent with the peak in CO. The match in timing of CO and NO_x suggests that the NO_x is primarily emitted in Metropolitan Sacramento and not downwind. The timing may also be an indicator of slowing photochemistry in the late evening. CO and NO_y observations in Sacramento during this same period exhibited a slope of 13.7 molecules CO per molecule NO_y (Sacramento-Del Paso Manor, ARB Site 34295; http://www.arb.ca.gov/adam). This slope is very similar to the CO:NO_x emission ratio of 15.4 reported for light-duty vehicles as measured in the Caldecott tunnel in the San Francisco Bay area the same year (Ban-Weiss et al., 2008). In comparison, a plot of the CO vs. NO_x concentrations observed at UC-BFRS for the peak

◄◄ | ►►

◄ | ►

Back | Close

Full Screen / Esc

Printer-friendly Version

Interactive Discussion

period (17–20 h) yields a slope of 50 CO per NO_x. Since nearly all the NO_y measured in Sacramento is NO_x, and since additional NO_x and CO sources (discussed in Sect. 4.1) are only of order 10–20% of the afternoon increase, this indicates that approximately 70% of the NO_x (not lost to dilution effects) was oxidized during the transport of the Sacramento plume to UC-BFRS. The corresponding CO vs. NO_y slope at UC-BFRS was 22 CO/NO_y indicating that of order 40% of the NO_y was lost to deposition during plume transport.

NO_x decreases rapidly, immediately after the 17–20 h peak, with a slower decrease after midnight. In contrast, CO concentrations decreased smoothly and continuously from 17–21 h until morning. The more rapid decrease in nighttime NO_x compared to CO is due to a combination of mixing with the low-NO_x background air (~50 ppt) and to chemical conversion of NO_2 to NO_3 and N_2O_5 at night. A calculation including NO_3 formation and subsequent N_2O_5 formation (in equilibrium with thermal decomposition) for a summer night at UC-BFRS predicts that ~70% of the NO_x will be converted to NO_3+N_2O_5 during an 8-h night in the NBL. Chemical losses of NO_3+N_2O_5 could account for nearly all of the nighttime decrease of NO_x from 0.9 ppb to 0.35 ppb. However, the air transported past this location during nighttime comes from further east. Although air upwind is affected by the urban plume, the degree is likely less and further dilution may have occurred, making it likely that several effects in addition to chemistry are responsible for the nocturnal decrease (see Sect. 5.1 for additional discussion).

NO displayed a broad maximum during daytime (~80 ppt) and a nearly constant minimum during nighttime (Fig. 4). During the day NO is produced by photolysis of NO_2 and is lost by reaction with ozone and peroxy radicals (RO_2 and HO_2). These photochemical reactions establish a photostationary-state that controls the concentration of NO relative to NO_2. The ratio of NO:NO_2 displays a broad mid-day maximum (~0.18). Differences in the diurnal patterns of NO and NO:NO_2 are used to elicit information about the local peroxy radical concentrations (see Sect. 5.3).

The secondary maximum in the morning exhibits peaks in NO, NO_2, and the NO/NO_2 ratio. Evidence that these are driven by dynamical mixing of the nocturnal boundary

and residual layers is presented in Sect. 5.2.

4.3 HNO_3

Transport of the Sacramento urban plume had less effect on the timing of the diurnal cycle of HNO_3 compared to the organic nitrates and NO_x (Fig. 4). The phase of the diurnal cycle is similar to that of sunlight and to temperature. We suggest that HNO_3 at this site is controlled by local production and rapid losses. HNO_3 production and losses are modeled as in Eq. (1) assuming chemical production, deposition, and dilution of HNO_3 are in steady state (Day et al., 2008):

$$k_{OH+NO_2}[OH][NO_2] = \frac{V_{dep}}{H_{ml}}[HNO_3] + K_{dil}([HNO_3]-[HNO_3]_{bg}) \tag{1}$$

Here V_{dep} is the deposition velocity (0.034 m/s (Farmer and Cohen, 2008)), H_{ml} is the mixed layer height ($\sim$800 m (Seaman et al., 1995; Carroll and Dixon, 1998; Dillon et al., 2002)), K_{dil} is the dilution rate constant representing both vertical venting and horizontal diffusion of the plume into the background air (0.31 h^{-1}; Perez and Cohen, 2009), and $[HNO_3]_{bg}$ is the background nitric acid concentration into which the plume is diluted. We estimate that the free-tropospheric $[HNO_3]_{bg}$ for this region is 200 ppt which is the intercept of $[HNO_3]$ vs. $[H_2O]$ for similar observations discussed in Murphy et al. (2006) made at a site at higher elevation in the Sierras where the sampling site was often affected by free tropospheric air.

Calculations using Eq. (1) predict daytime HNO_3 concentrations have a shape similar to that of OH and to the variation in solar insolation (e.g. Brown et al., 2004). The observed diurnal cycles are consistent with this prediction.

At night, when OH concentrations are much lower, the OH source term approaches zero and HNO_3 concentrations should be controlled by deposition and decrease to a small fraction of daytime values. However, the HNO_3 decreased less than expected and remained relatively constant at night. This observation suggests local HNO_3 production through NO_3 and N_2O_5 formation and subsequent reactions and/or continued

downward mixing of residual layer air are occurring at night. However, downward mixing of air would likely bring PNs with it, which would be inconsistent with observations of decreasing ΣPNs throughout the night at UC-BFRS. Nighttime N_2O_5-driven HNO_3 production has been invoked to explain substantial fluxes of NO_y at night (1996; Munger et al., 1998) and observations of elevated HNO_3 and depressed N_2O_5 at night (Brown et al., 2004). Our observations are consistent with the presence of an additional source of HNO_3 as discussed in more detail in Sect. 5.1.

For summertime mid-day concentrations of 0.5 ppb NO_2 and 1 ppb HNO_3 (and average boundary layer temperatures and gas density based on a mid-day surface temperature of 24°C) we use Eq. (1) to calculate an OH concentration of 2.1×10^7 molecules cm^{-3}, approximately double that of the integrated value in the Sacramento plume of 1.1×10^7 molecules cm^{-3} calculated by Dillon et al. (2002). The lifetime of HNO_3 to the combination of deposition and dilution is ~2.2 h. Therefore, much of the HNO_3 observed at UC-BFRS may be produced upwind. Moreover, concentrations of NO_x and OH two hours upwind are two to three times higher than observed at UC-BFRS, respectively (Murphy et al., 2007), suggesting that HNO_3 production may be occurring much more rapidly upwind. Consequently, these factors imply that not only is the OH calculated using Eq. (1) probably more representative of the integrated OH a few hours upwind, but furthermore is biased high due to the underestimate of NO_2 concentrations that are relevant to conditions where the HNO_3 was produced. This factor likely explains the high OH estimate compared to that of Dillon et al. (2002). Detailed time dependent model calculations support this idea and suggest an average OH of 5.0×10^6 molecules cm^{-3} (Perez and Cohen, 2009).

The rapid decrease of HNO_3 at sunset (18–21 h) is consistent with a short lifetime (~2.2 h), however, it might be expected that when the OH value drops significantly (likely shortly after solar noon), the HNO_3 concentration would decrease on this timescale. As observed in Fig. 4, a rapid decrease does not occur until hour 18. The ratio HNO_3/NO_2, shown in Fig. 5, does peak at solar noon and displays a rapid decrease starting after hour 16. This indicates the lag in HNO_3 concentrations is due to

increased NO_2 and no unusual chemistry.

Another interesting feature in the diurnal cycle of HNO_3 is the absolute minimum and local minimum in HNO_3/NO_2 near sunrise and sunset (Fig. 5), the transition period between daytime and nighttime chemistry. Brown et al. (2004) observed similar features in their observations of HNO_3 which they attribute to the dusk/dawn transition period when there is insufficient sunlight to drive significant production of OH but sufficient sunlight to produce enough NO from NO_2 photolysis to suppress NO_3 concentrations.

The diurnal cycle of HNO_3 at UC-BFRS is similar to observations at other sites and indicates that transport is less important as a control over HNO_3 than for CO and other NO_y species at the site. Lefer et al. (1999) report a similar diurnal cycle for summertime measurements of HNO_3 at Harvard Forest, where median values reached 2 ppb at midday and dropped to 400–700 ppt at night for the more polluted wind sector. For the cleaner wind sector, a much smaller amplitude cycle was observed (150 ppt at night, 300 ppt during daytime). Horii (2002) reported similar diurnal cycles for another summer at Harvard Forest although the amplitude for the polluted sector data was less than reported by Lefer et al. (1999). For a mountain site, Niwot Ridge, Colorado, Parrish et al. (1986) show a similar diurnal cycle that, on average, peaked around 350 ppt and dropped to ~80 ppt at night during the summer. They also report that, on average, HNO_3 concentrations and both the observed and modeled HNO_3/NO_x ratio peaked a few hours after noon. Kleinman et al. (1994) show HNO_3 observations from a site in rural Georgia with a very similar diurnal cycle to our summer data with nighttime values of ~300 ppt and a daytime peak of ~1 ppb. Brown et al. (2004) describe HNO_3 measurements for the relatively polluted marine boundary layer off the eastern US coast and observe that HNO_3 peaks near midday at nearly 2 ppb and persists at 0.5–1 ppb during nighttime.

⏮ | ⏭

◀ | ▶

Back | Close

Full Screen / Esc

Printer-friendly Version

Interactive Discussion

4.4 ΣPNs

ΣPNs are approximately in thermal equilibrium with peroxyacyl radicals (PA_i) and NO_2 under warm boundary layer conditions:
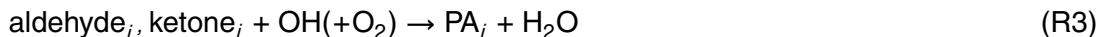
$$K_{PN_i}(T) = \frac{[PN_i]}{[PA_i][NO_2]} \tag{2}$$

where $K_{PN_i}(T)$ is the equilibrium constant for each respective PN. This equilibrium is established through the reactions:

$$PA_i + NO_2 \rightarrow PN_i \tag{R1}$$
$$PN_i \rightarrow PA_i + NO_2 \tag{R2}$$

5 which determine the partitioning of the PN reservoir between the stable PN_i and its radical partner, PA_i. In addition, peroxyacyl radicals are also approximately in photo-chemical steady-state with their sources and sinks (Cleary et al., 2007; LaFranchi et al., 2009).

The primary reactions that contribute to net formation and loss of the sum of a PA_i and PN_i ($PN_{Ti} \equiv PA_i + PN_i$) include:

$$aldehyde_i, ketone_i + OH(+O_2) \rightarrow PA_i + H_2O \tag{R3}$$
$$PA_i + NO \rightarrow Products \tag{R4}$$
$$PA_i + HO_2 \rightarrow Products \tag{R5}$$
$$PA_i + RO_2 \rightarrow Products \tag{R6}$$
$$PN_i + OH \rightarrow Products \tag{R7}$$

Since Reaction (R7) will have a small effect for most PN molecules, we neglect it and
10 solve for the steady-state concentration of PN_{Ti} and derive:

$$[PN_{Ti}]_{ss} = \frac{k_3[aldehyde_i][OH]}{k_4[NO] + k_5[HO_2] + k_6[RO_2]}(1 + K_{PN_i}[NO_2]) \tag{3}$$

3453

This relationship is similar to that derived by Cleary et al. (2007) with the addition of peroxy radical reactions which are important sinks of PA radicals at UC-BFRS but were not in the region studied by Cleary et al. (2007) At UC-BFRS, noontime NO was observed to be 80 ppt and the [HO_2+RO_2] was calculated to be ~160 ppt (Sect. 4.4). If we approximate that RO_2 is equal to HO_2 and use the reaction rate constant of $CH_3C(O)O_2$+CH_3O_2 for Reaction (R6), the net contribution of Reactions (R5) and (R6) to PA$_i$ destruction is calculated to be 1.3 times that of Reaction (R4).

At UC-BFRS, ΣPNs peaked at 17 h in the afternoon and decreased continuously through the night until about 6–10 h, at which point they began to increase (Fig. 4). The rapid rise in ΣPNs of 50% in late morning (from 0.5 to 0.75 ppb @ 9–11 h) is concurrent with a comparable 45% increase in acetaldehyde from 0.43 to 0.62 ppb (data not shown). If the majority of ΣPNs consisted of peroxyacetyl nitrate (PAN) and acetaldehyde constituted the principal source of PAN then, according to Eq. (3), the increase in acetaldehyde could explain the morning rise in ΣPNs. However, as shown in Eq. (3), several other factors control the PNs concentrations in this steady-state approximation. During this morning rise, [HO_2+RO_2] and temperature increase, both acting as negative forcing on ΣPNs concentrations, whereas NO_2, OH, and acetaldehyde increase, all of which would work to increase ΣPNs. The combined effect of these shifts, in addition to changes in the other aldehyde molecules that are precursors to PA$_i$ radicals, account for the observed ΣPNs mid-day profile.

Using average noontime concentrations and temperatures (Figs. 3 and 4), approximating that PAN comprises 80% of ΣPNs (Cleary et al., 2007) and that acetaldehyde is the sole source of PAN, we use Eq. (3) to calculate that the noontime OH concentration is 1.5×10^7 molecules cm^{-3}. This is very similar to the 2.1×10^7 molecules cm^{-3} calculated in Sect. 4.3 using the photo-stationary state approximation for HNO_3 and NO_2. However, as discussed, that calculation may substantially overestimate local OH concentrations in part because it reflects the integrated OH concentrations between UC-BFRS and a couple hours upwind where OH concentrations are likely higher by a factor of 2–3.

It has been suggested that in regions heavily influenced by isoprene oxidation that an additional source of peroxyacetyl radicals, as much as 3-fold that of acetaldehyde, are necessary to explain observed PAN levels (Roberts et al., 2001; Cleary et al., 2007). Methylglyoxal (MGLY) has been suggested as a possible identity of this additional source (Romero et al., 2005). If we invoke additional sources of PAN that are 3 times larger than the acetaldehyde source, we calculate a 4-fold lower OH (3.8×10^6 molecules cm^{-3}). The rapid rise in ΣPNs in late morning is concurrent with the timing of morning increases in isoprene, methyl vinyl ketone (MVK), and methacrolein (MACR) (Dreyfus et al., 2002). This is consistent with isoprene oxidation accounting for an additional source of PAN in the region. In a recent study, using a more complete suite of VOC observations and three speciated acyl peroxy nitrate compounds at UC-BFRS, LaFranchi et al. (2009) calculate that non-acetaldehyde sources (MGLY, MACR, MVK, and biacetyl) account for ~3 times that from acetaldyde for the production of PAN for average midday temperatures observed in this study (24°C). MVK represented the majority of those other sources and they demonstrated a closure of the peroxy acetyl (PA) radical budget. These additional acyl peroxy radical production sources are all proportional to OH concentrations (except biacetyl which was <10% of PA production), confirming that OH of approximately 4×10^6 molecules cm^{-3} is a more accurate estimate for local noontime OH concentrations than the higher estimates based on acetaldehyde alone.

The initial component of the evening decrease in ΣPNs coincides with decreases in isoprene, MVK, and MACR (but not acetaldehyde). ΣPNs continue to decrease gradually throughout the night to 50% of their mixing ratio at 6 h. We estimate a lower bound on the nighttime chemical loss rate in the absence of NO by assuming PA radicals are formed through ΣPN decomposition (R2) and that PA_i–PA_i self reactions are the only important sink. For typical nighttime ΣPNs (0.7 ppb), NO_2 (0.5 ppb), and temperature (16°C), we estimate approximately 0.6 ppt ΣPA_i and 1% loss of ΣPNs over an 8-h night. The ~40% decrease we observe from 20 to 4 h would be consistent with $[RO_2+HO_2]$ levels ~20 times higher (10 ppt) and would result in a NO_x source of ~200 ppt. Losses

of ΣPNs are also due to reaction with soil NO emissions and surface deposition.

4.5 ΣANs
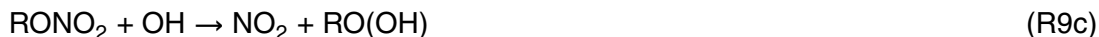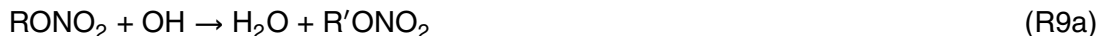
ΣANs peaked at 20 h along with other chemicals transported in the Sacramento plume and were lowest in the morning (minima at 5 and 10 h) (Fig. 4).

ΣANs are formed through the minor channel of the reaction of organic peroxy radicals with NO:

$$RO_2 + NO \rightarrow RO + NO_2 \tag{R8a}$$
$$RO_2 + NO \rightarrow RONO_2 \tag{R8b}$$
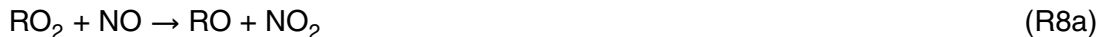
5 Reaction (R8a) typically leads to the formation of 2 ozone molecules, whereas Reaction (R8b) results in formation of an alkyl nitrate. Depending on the R-group the branching ratio can range from one percent to tens of percent. The effective branching ratio for the mixture of VOC present at UC-BFRS (Day et al., 2003) and Granite Bay, CA ($\sim$4 h upwind) (Cleary et al., 2005) has been inferred from the ΣANs correlation
10 with O_3 to be $\sim$2.5% and $\sim$4%, respectively.

Losses of ΣANs within the boundary layer can occur though both dry deposition and through reaction with OH. The deposition velocity for ΣANs was calculated to be 0.027 m/s during summer, nearly 80% that of HNO_3 (Farmer and Cohen, 2008). This suggests that the stickier hydroxyalkyl nitrates make up a significant fraction of ΣANs. For a daytime boundary layer of 800 m this corresponds to a lifetime to deposition of $\sim$8 h. The most important chemical reaction for ANs during the day, reaction with OH, can result in products that retain the organic nitrate functionality (Reaction R9a) or that convert the nitrogen either to HNO_3 or NO_2 (see Perring et al., 2008, for additional discussion):

$$RONO_2 + OH \rightarrow H_2O + R'ONO_2 \tag{R9a}$$
$$RONO_2 + OH \rightarrow HNO_3 + R'O \tag{R9b}$$
$$RONO_2 + OH \rightarrow NO_2 + RO(OH) \tag{R9c}$$

Farmer et al. (2008) estimate the ΣAN loss branches (R9b and R9c) comprise 6–30% of the net rate of Reaction (9). For OH of 5×10^6 molecules cm^{-3} and a rate constant for Reaction (9) of 4.57×10^{-11} molecules cm^{-3} s^{-1} (Horowitz et al., 2007), this corresponds to a lifetime of 4–20 h for reactive nitrogen in the form of ΣANs (but not necessarily as the original molecular structure). This is a chemical lifetime comparable to the deposition lifetime.

A variety of diurnal behaviors have been reported for ΣANs. Buhr et al. (1990) report measurements of C_2-C_5 mono-functional alkyl nitrates and observed that ΣANs increased in the morning with the nocturnal boundary layer break-up (concurrent with NO_y increases), remained relatively constant throughout the day, followed by a slow decline at night within the nocturnal boundary layer. Flocke et al. (1998) report measurements of more than 20 different C_1-C_8 mono-functional alkyl nitrates for Schauinsland, Germany. During summer, total alkyl nitrates approximately doubled between 9 and 14 h, concurrently with upslope flow from a polluted urban region and increases of NO_y and O_3, and then decreased from evening to the morning. O'Brien et al. (1995) report four days of observations during August at a site in rural Ontario where they measured twelve C_3-C_6 mono-functional alkyl nitrates, four C_2-C_4 hydroxyalkyl nitrates, and one alkyl di-nitrate. No diurnal cycle was apparent in total or hydroxyalkyl nitrates. In contrast, O'Brien et al. (1997) describe a month-long experiment where a similar suite of alkyl nitrates was measured 50 km from Vancouver, B.C. and show that total, total mono-functional-, and total hydroxyalkyl nitrates (and an unidentified alkyl nitrate component) had a large diurnal cycle peaking in early afternoon. Peak daytime values were 5–10 times the nighttime minima. They suggest that that the bulk of alkyl nitrates were locally produced and that isoprene nitrates may be an important component of alkyl nitrates at this site. At the PROPHET site, Grossenbacher et al. (2001) report measurements of isoprene nitrates that showed a clear diurnal cycle peaking in early afternoon around 10 ppt and decreasing to a 1–2 ppt at night. For the same period at this site, C_3-C_5 mono-functional alkyl nitrates were measured and did not display any consistent diurnal cycle (Ostling et al., 2001). In another experiment, in rural

Tennessee (Southern Oxidants Study 1999), isoprene nitrates were observed to have a similar diurnal cycle but at 5–10 times the concentrations with an average mid-day peak of 115 ppt (5–10 ppt nighttime minimum) (Grossenbacher et al., 2004). Our own summer measurements at Granite Bay, California and La Porte, Texas exhibited diurnal
5 cycles that varied by a factor of two or four (respectively) between day and night, suggesting that sources were local. The diurnal cycle of ΣANs at UC-BFRS most closely follows that described by Flocke et al. (1998) where daily flow patterns had a stronger influence than local photochemistry.

The diurnal cycle of ΣANs can be contrasted to ΣPNs, which peaked earlier and by
10 a greater factor over the morning mixing ratios lows. The observation that ΣANs peaked later during the day than ΣPNs suggests that the isoprene-related source, originating in the foothills, is a bigger fraction of the ΣPN sources than it is for the ΣAN sources. During the nighttime through late-morning ΣPNs and ΣANs display a similar pattern, decreasing by a similar relative magnitude with a small increase in mid-morning. There
15 is much greater variability in ΣPNs during afternoon (as illustrated by the 68th percentile bounds in Fig. 4). This is due to synoptic timescale temperature effects that affect PNs more strongly than ANs (Day et al., 2008).

To understand the implications of the different relative magnitudes of the diurnal patterns, we compare the various production and loss processes that affect these two
20 compound classes during the daytime. We estimate that the free-tropospheric backgrounds of ΣPNs and ΣANs for this region are <50–100 ppt, calculated from the intercept of the respective compound class vs. [H_2O] for similar observations higher in the Sierras discussed in Murphy et al. (2006). Since both ΣANs and ΣPNs do not decrease below 350–400 ppt during their morning minima, much higher than their background
25 values, subtle differences in their backgrounds cannot explain significant differences in their diurnal patterns. However, the deposition velocity for ΣANs has been shown to be 2.5 times greater than for ΣPNs at this site. Therefore, differing deposition rates may partly explain the larger relative increase that ΣPNs experience during midday, as deposition of ΣANs acts to depress concentrations. Increases in OH will also act

as a larger direct positive forcing on ΣPNs concentrations since although the production of both are roughly proportional to OH, ΣANs have significant OH-mediated losses (Reactions R9b and R9c).

Qualitatively we observe that the period where transport and production result in a net increase of observed ΣPNs occurs over a shorter time period (10–17 h) than for ΣANs (10–21 h). After 17 h, ΣPNs decrease. Likely, net chemical production of both ΣPNs and ΣANs is slowing at this time of day. However if ΣANs and its precursor VOCs have a larger contribution from within the Sacramento urban plume compared to ΣPNs, the increasing impact of the plume during this period (17–20 h) could drive the gradual increase in ΣANs observed. In effect, this explanation characterizes the ΣPNs production as being more concentrated in a smaller band of the plume (due to the line source of BVOC emissions between UC-BFRS and Sacramento) whereas ΣANs sources are distributed more evenly throughout the plume (due to a mixture of biogenic and anthropogenic VOC sources). Also, a broad range of mono and sesquiterpenes are known to be emitted from the plants at this site (Bouvier-Brown et al., 2008) and their oxidation likely leads to terpene nitrates. This more local source of ΣANs is also consistent with a more temporally diffuse source during the daytime, possibly transitioning into nighttime ΣANs production through reactions with NO_3.

5 Combined analyses

5.1 Nocturnal chemistry

Combining the constraints from our observations of NO, NO_2, ΣPNs, ΣANs, HNO_3, and O_3 provides additional insight into nocturnal chemistry. As described above, invoking NO_3 and N_2O_5 chemistry is necessary to describing the nighttime NO_x decrease. We calculate that at aerosol surface area typical of UC-BFRS, N_2O_5 reactions are too slow to compete with NO_3+VOC reactions.

Reactions of NO_3 with biogenic VOC (BVOC) and aldehydes:

$$NO_3 + RH_2RH_2 \rightarrow \text{Products}(RONO_2, NO_x, HNO_3\ldots) \tag{R10}$$

$$NO_3 + RH \rightarrow HNO_3 \tag{R11}$$
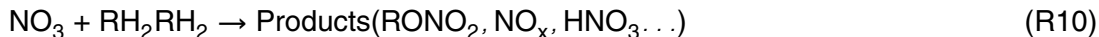
are rapid and are an estimated 90% of the combined loss of $NO_3 + N_2O_5$. These reactions are a source of the sustained nighttime HNO_3 concentrations and also a source of ANs.

⁵ As a first step toward a quantitative description of the nocturnal reactive nitrogen chemistry at UC-BFRS, we applied a chemical box model to calculate the temporal evolution of O_3, NO_2, NO_3, N_2O_5, ΣPNs, ΣANs, and HNO_3 at night for typical conditions at UC-BFRS and upwind. The model included 21 important nighttime NO_x and HO_x reactions in addition to VOC reactions that were limited to isoprene, α-pinene, β-pinene, and 3-carene reactions with OH, O_3, and NO_3 and reactions of aldehydes ¹⁰ (as one chemical group) with OH and NO_3.

The model was initialized with observations from Big Hill, CA at 9 p.m. (Murphy et al., 2006). Big Hill is 20 km (~8 h at nighttime wind speeds) upwind of UC-BFRS. We then compare the model to observations at 5 a.m. from UC-BFRS (Figs. 3 and 4). Initial concentrations of O_3, NO_2, ΣANs, ΣPNs, HNO_3 were 61, 0.41, 0.50, 0.49, and ¹⁵ 0.51 ppb, respectively (see Murphy et al., 2006, Figs. 13 and 14).

The nocturnal boundary layer was assumed to be 100 m deep. The aldehyde and BVOC concentrations at Big Hill were estimated to be 70% of concentrations observed or calculated at UC-BFRS (Lamanna and Goldstein, 1999; Schade et al., 1999a; Lee et al., 2005; Holzinger et al., 2006; Perez, 2008). Deposition rates were estimated by ²⁰ assuming that no dilution occurs as the air is transported from Bill Hill to UC-BFRS and the decrease in O_3 is due solely to deposition. This resulted in a deposition velocity of ~5% that of daytime values (~0.6 cm/s, Bauer et al., 2000), a realistic drop for low turbulence nighttime conditions (Finkelstein et al., 2000; Farmer and Cohen, 2008). Daytime deposition velocities of ΣANs, ΣPNs and HNO_3 (2.7, 1.1, 3.4 cm/s), reported ²⁵ by Farmer and Cohen (2008) were scaled by this same factor.

3460

Printer-friendly Version

Interactive Discussion

Reactions of NO_3 with aldehydes were assumed to produce HNO_3 with a 95% yield and NO_2 with a 5% yield. The overall contribution to HNO_3 production via aldehyde reactions was small. However, reaction of NO_3 with BVOC (at UC-BFRS: alpha-pinene (140 ppt), beta-pinene (200 ppt), 3-carene (80 ppt), isoprene (600 ppt)), had strong control over NO_x, HNO_3, and ΣANs. The relative yields of HNO_3, ΣANs, and NO_2 was tuned along with soil NO_x emissions (to compensate for deposition losses) to exactly match NO_2, HNO_3, and ΣANs concentrations at UC-BFRS at 5 a.m. This resulted in an estimate for the branching ratio of BVOC+NO_3 of 45% HNO_3, 25% ANs, and the remainder NO_2. Soil emissions were 1.3 ppt m s^{-1}, approximately 10% that of the daytime emissions calculated by Farmer and Cohen (2008).

The 25% yield of ΣANs is not to be interpreted as the effect of a primary reaction, but rather as the effective yield over 8 h. Some ΣANs may react quickly and be returned to the pool of other N species. We did not attempt to represent these details in this simple model. Clearly, a better representation of the nighttime reactive nitrogen chemistry will require an improved understanding of the branching ratio of BVOC+NO_3 reactions.

5.2 Morning chemistry and boundary layer dynamics

At approximately 06:00 in the morning, at or just before both sunrise and the downslope/upslope wind shift, the concentrations of some species were observed to increase rapidly. This is earlier than can be explained by horizontal transport. The timing of these changes coincides with the timing of a rapid decrease in O_3 mixing ratios, which has been attributed to a morning stomatal opening in response to sunlight that causes rapid O_3 deposition in the shallow nocturnal boundary layer (Bauer et al., 2000; Kurpius et al., 2002).

Rather than a stomatal process, the NO_{yi} changes are likely the result of boundary layer dynamics. The NO_x rise is likely the result of the break-up of the nocturnal boundary layer, mixing down air from the residual layer that is less depleted in NO_x having experienced less surface deposition and exposed to lower VOC concentrations and therefore less loss through NO_3 and N_2O_5 reactions. Further, even slight heating

at the surface would cause convection of nighttime soil NO emissions and contribute to increased NO_x. Stomatal NO emissions have been observed from coniferous trees (Wildt et al., 1997) but are unlikely to be large enough to cause the observed mixing ratio trend. More likely, the larger relative rise in NO as compared to the NO_2 is due to the O_3 decrease (see Sect. 5.3). Similar observations of NO_x and a presumed connection to break-up of the nocturnal inversion have been reported for measurements at Scotia, PA (Buhr et al., 1990), Harvard Forest (Munger et al., 1996), and Northern Michigan (Thornberry et al., 2001).

HNO_3 typically increased rapidly in the morning starting around hours 6–7, and then was constant or dipped for a few hours before continuing to increase through early afternoon (Figs. 2 and 4). This sharp morning rise preceded the expected rise in OH concentrations and was coincident with the early morning peaks in NO, NO_2, and ΣPNs and with the dip or recovery of O_3 from its morning minimum. This feature is similar to observations at other sites during summer. Lefer et al. (1999), Kleinman et al. (1994), and Trainer et al. (1991) point out that the sharp rise in diurnal observations of HNO_3 occurs earlier in the morning than they would expect based on the expected OH profile, but is consistent with the breakup of the nocturnal boundary layer and mixing of higher HNO_3 concentrations from above.

A slight peak in both ΣANs and ΣPNs also occurs in the morning, concurrent or slightly after the NO_x peak and is consistent with the nocturnal boundary layer breakup and mixing down of air less depleted in organic nitrates. Although this feature in ΣPNs is not reported for other sites possessing a morning NO_x peak or early HNO_3 rise, many authors (Shepson et al., 1992; Bottenheim et al., 1994; Roberts et al., 1995; Aneja et al., 1996; Thornberry et al., 2001) have attributed the early morning rise in PAN to breakup of the nocturnal boundary layer with subsequent increases due to photochemical production obscuring an early morning peak as is observed for NO_x. A similar peak was observed for CO which may be the result of more rapid soil emissions of CO following a nighttime build-up initiated by rising temperatures or increased sunlight photolyzing aldehydes that accumulated overnight.

5.3 Peroxy radicals

NO concentrations are approximately in steady state with NO_2 during daylight. The ratio of NO/NO_2 is inversely proportional to O_3 and to the $NO+O_3$ rate constant and proportional to the NO_2 photolysis rate constant. In the absence of local NO_x emissions or peroxy radicals (HO_2, RO_2), the relationship between NO and NO_2 is governed by the following reactions:

$$NO_2 + h\nu \rightarrow NO + O \tag{R12}$$
$$NO + O_3 \rightarrow NO_2 + O_2 \tag{R13}$$

Under these conditions, the photostationary-state approximation yields:

$$[NO]/[NO_2] = \frac{j_{12}}{k_{13}[O_3]} \tag{4}$$

Although peroxy radicals may often be only 10's of ppt in rural locations they react rapidly with NO (the rate constant is 100 times faster than for the $NO+O_3$ reaction) converting it to NO_2:

$$HO_2 + NO \rightarrow NO_2 + OH \tag{R14}$$

$$RO_2 + NO \rightarrow NO_2 + RO \tag{R8a}$$

This additional conversion of NO to NO_2 is commonly represented as a deviation from photostationary state (as defined by R12 and R13) with the equation:

$$\phi = \frac{j_{12}[NO_2]}{[O_3]k_{13}[NO]} \tag{5}$$

In the absence of NO_x sources (such that steady-state is achieved), ϕ is unity at $[HO_2+RO_2]=0$. ϕ increases with increasing $[HO_2+RO_2]$. In Fig. 6, the calculated diurnal cycle of ϕ is shown. By midday ϕ is 2–3, suggesting the presence of large peroxy

Title Page

Abstract | Introduction

Conclusions | References

Tables | Figures

◄ | ►►

◄ | ►

Back | Close

Full Screen / Esc

Printer-friendly Version

Interactive Discussion

radical concentrations and indicating that peroxy radicals are more important to conversion of NO to NO_2 than is reaction with O_3. Including Reactions (R14) and (R8a) in the photostationary-state model yields an equation with which to estimate $[HO_2+RO_2]$ concentrations:

$$[HO_2 + RO_2] = \frac{1}{k_{14}(j_{12}\frac{[NO_2]}{[NO]} - k_{13}[O_3])} \tag{6}$$

where k_{14} is used for the rate constant of both Reactions (R14) and (R8a) since the rate constants are similar. The average diurnal cycle of $[HO_2+RO_2]$, derived from Eq. (6), is shown in the bottom panel of Fig. 6.

The concentrations of $[HO_2+RO_2]$ reach 200 ppt. These values are 2–8 times higher than other measurements or modeled values at rural, urban, and remote sites where they have typically been reported to have midday peaks of 25–100 ppt (Cantrell et al., 1996a,b; Hauglustaine et al., 1996; Cantrell et al., 1997; Thornton et al., 2002; Mihele and Hastie, 2003). Such high peroxy radical concentrations suggest significant local oxidation of VOCs, either by OH or O_3. For observed mid-afternoon NO_x and O_3 concentrations, a VOC reactivity of $8\,s^{-1}$ [OH], [OH]=5×10^6 molecules cm^{-3}, and using a photostationary state model, we calculate $RO_2 \sim HO_2 \sim 100$ ppt. This is consistent with the high $[RO_2+HO_2]$ we calculate from a NO-NO_2-O_3 photostationary state model and compared to other observations, is attributable to the combination of relatively low NO_x and high VOC reactivity conditions. A doubling of OH yields a calculated 50% increase in $[RO_2+HO_2]$, therefore an average mid-day OH concentration of 5×10^6 molecules cm^{-3} is most consistent with the observed NO_x–HO_x chemistry.

6   Conclusions

We describe diurnal cycles in summertime observations of ΣNO_{yi}, NO_2, NO, ΣPNs, ΣANs, and HNO_3 at a forested, mid-elevation site in the Sierras affected daily by the

Summertime diurnal cycles of NOyi

D. A. Day et al.

Title Page

Abstract | Introduction

Conclusions | References

Tables | Figures

◄ | ►

◄ | ►

Back | Close

Full Screen / Esc

Printer-friendly Version

Interactive Discussion

Sacramento urban plume. The shifts in the timing and relative amplitudes of the diurnal cycles of different NO_{yi} species and the partitioning of NO_z are attributed to various differences in photochemical production rates, lifetimes, and direct and precursor emission source locations. The diurnal cycle of HNO_3 was primarily driven by local photochemistry. The diurnal cycles of ΣPNs and ΣANs were largely driven by production and transport within the Sacramento plume, with strong indications that, by comparison, the former has a larger contribution of biogenic VOC precursors.

Daytime peroxy radical concentrations were calculated to be larger than most previous observations, providing evidence for highly oxidizing conditions and favorable conditions for large alkyl nitrate production. Nighttime concentrations of different nitrogen species are driven by a combination of deposition and chemistry, with strong evidence for large nighttime HNO_3 and ΣANs production via NO_3+alkenes.

References

Aneja, V. P., Kim, D. S., Das, M., and Hartsell, B. E.: Measurements and analysis of reactive nitrogen species in the rural troposphere of Southeast United States: Southern oxidant study site SONIA, Atmos. Environ., 30, 649–659, 1996.

Ban-Weiss, G. A., McLaughlin, J. P., Harley, R. A., Lunden, M. M., Kirchstetter, T. W., Kean, A. J., Strawa, A. W., Stevenson, E. D., and Kendall, G. R.: Long-term changes in emissions of nitrogen oxides and particulate matter from on-road gasoline and diesel vehicles, Atmos. Environ., 42, 220–232, doi:10.1016/j.atmosenv.2007.09.049, 2008.

Bauer, M. R., Hultman, N. E., Panek, J. A., and Goldstein, A. H.: Ozone deposition to a pon-derosa pine plantation in the Sierra Nevada Mountains (CA): a comparison of two different climatic years, J. Geophys. Res., 105, 22123–22136, 2000.

Bertram, T. H. and Cohen, R. C.: A prototype instrument for the real time detection of semi-volatile organic and inorganic nitrate aerosol, Eos Trans. AGU, 84(46), Fall Meet. Suppl., San Francisco, USA, 8–12 December 2003, A51F-0740, 2003.

Bottenheim, J. W., Sirois, A., Brice, K. A., and Gallant, A. J.: Five years of continuous ob-servations of PAN and ozone at a rural location in eastern Canada, J. Geophys. Res., 99, 5333–5352, 1994.

Bouvier-Brown, N. C., Holzinger, R., Palitzsch, K., and Goldstein, A. H.: Large emissions of sesquiterpenes and methyl chavicol quantified from branch enclosure measurements, At-mos. Environ., 43, 389–401, doi:10.1016/j.atmosenv.2008.08.039, 2009.

Brown, S. S., Dibb, J. E., Stark, H., Aldener, M., Vozella, M., Whitlow, S., Williams, E. J., Lerner, B. M., Jakoubek, R., Middlebrook, A. M., DeGouw, J. A., Warneke, C., Goldan, P. D., Kuster, W. C., Angevine, W. M., Sueper, D. T., Quinn, P. K., Bates, T. S., Meagher, J. F., Fehsenfeld, F. C., and Ravishankara, A. R.: Nighttime removal of NO_x in the summer marine boundary layer, Geophys. Res. Lett., 31, L07108, doi:10.1029/2004GL019412, 2004.

Buhr, M. P., Parrish, D. D., Norton, R. B., Fehsenfeld, F. C., Sievers, R. E., and Roberts, J. M.: Contribution of organic nitrates to the total reactive nitrogen budget at a rural eastern U.S. site, J. Geophys. Res., 95, 9809–9816, 1990.

Cantrell, C. A., Shetter, R. E., and Calvert, J.: Peroxy radical chemistry during FIELDVOC 1993 in Brittany, France, Atmos. Environ., 30, 3947–3957, 1996a.

Cantrell, C. A., Shetter, R. E., Gilpin, T. M., Calvert, J. G., Eisele, F. L., and Tanner, D. J.: Peroxy radical concentrations measured and calculated from trace gas measurements in the Mauna Loa observatory photochemistry experiment 2, J. Geophys. Res., 101, 14653–14664, 1996b.

Cantrell, C. A., Shetter, R. E., Calvert, J. G., Eisele, F. L., Williams, E., Baumann, K., Brune, W. H., Stevens, P. S., and Mather, J. H.: Peroxy radicals from photostationary state deviations and steady state calculations during the Tropospheric OH Photochemistry Experiment at Idaho Hill, Colorado, 1993, J. Geophys. Res., 102, 6369–6378, 1997.

Carroll, J. J. and Dixon, A. J.: Tracking the Sacramento pollutant plume over the western Sierra Nevada, Contract #94-334 Final Report, California Environmental Protection Agency Air Re-sources Board, 26 pp., available at: http://www.arb.ca.gov/research/apr/past/atmospheric.

htm, 1998.

Chen, X. H., Hulbert, D., and Shepson, P. B.: Measurement of the organic nitrate yield from OH reaction with isoprene, J. Geophys. Res., 103, 25563–25568, 1998.

Chuong, B. and Stevens, P. S.: Measurements of the kinetics of the OH-initiated oxidation of isoprene, J. Geophys. Res., 107, 4162, doi:10.1029/2001jd000865/issn0148-0227, 2002.

Cleary, P. A., Murphy, J. G., Wooldridge, P. J., Day, D. A., Millet, D. B., McKay, M., Goldstein, A. H., and Cohen, R. C.: Observations of total alkyl nitrates within the Sacramento Urban Plume, Atmos. Chem. Phys. Discuss., 5, 4801–4843, 2005, http://www.atmos-chem-phys-discuss.net/5/4801/2005/.

Cleary, P. A., Wooldridge, P. J., Millet, D. B., McKay, M., Goldstein, A. H., and Cohen, R. C.: Observations of total peroxy nitrates and aldehydes: measurement interpretation and inference of OH radical concentrations, Atmos. Chem. Phys., 7, 1947–1960, 2007, http://www.atmos-chem-phys.net/7/1947/2007/.

Day, D. A., Wooldridge, P. J., Dillon, M. B., Thornton, J. A., and Cohen, R. C.: A thermal dissociation laser-induced fluorescence instrument for in situ detection of NO_2, peroxy nitrates, alkyl nitrates, and HNO_3, J. Geophys. Res., 107, 4046, doi:10.1029/2001JD000779, 2002.

Day, D. A., Dillon, M. B., Wooldridge, P. J., Thornton, J. A., Rosen, R. S., Wood, E. C., and Cohen, R. C.: On alkyl nitrates, O_3, and the 'missing NO_y', J. Geophys. Res., 108, 4501, doi:10.1029/2003JD003685, 2003.

Day, D. A., Wooldridge, P. J., and Cohen, R. C.: Observations of the effects of temperature on atmospheric HNO_3, ΣANs, ΣPNs, and NO_x: evidence for a temperature-dependent HO_x source, Atmos. Chem. Phys., 8, 1867–1879, 2008, http://www.atmos-chem-phys.net/8/1867/2008/.

Dillon, M. B.: The chemical evolution of the Sacramento urban plume, PhD thesis, Department of Chemistry, University of California, Berkeley, 206 pp., 2002.

Dillon, M. B., Lamanna, M. S., Schade, G. W., Goldstein, A. H., and Cohen, R. C.: Chemical evolution of the Sacramento urban plume: Transport and oxidation, J. Geophys. Res., 107, 4045, doi:10.1029/2001JD000969, 2002.

Dreyfus, G. B., Schade, G. W., and Goldstein, A. H.: Observational constraints on the contribution of isoprene oxidation to ozone production on the western slope of the Sierra Nevada, CA, J. Geophys. Res., 107, 4365, doi:10.1029/2001JD001490, 2002.

Farmer, D. K., Wooldridge, P. J., and Cohen, R. C.: Application of thermal-dissociation laser induced fluorescence (TD-LIF) to measurement of HNO_3, Σalkyl nitrates, Σperoxy nitrates,

and NO_2 fluxes using eddy covariance, Atmos. Chem. Phys., 6, 3471–3486, 2006, http://www.atmos-chem-phys.net/6/3471/2006/.

Farmer, D. K. and Cohen, R. C.: Observations of HNO_3, ΣAN, ΣPN and NO_2 fluxes: evidence for rapid HOx chemistry within a pine forest canopy, Atmos. Chem. Phys., 8, 3899–3917, 2008, http://www.atmos-chem-phys.net/8/3899/2008/.

Finkelstein, P. L., Ellestad, T. G., Clarke, J. F., Meyers, T. P., Schwede, D. B., Hebert, E. O., and Neal, J. A.: Ozone and sulfur dioxide dry deposition to forests: Observations and model evaluation, J. Geophys. Res., 105, 15365–15377, 2000.

Fischer, M. L. and Littlejohn, D.: Ammonia at Blodgett Forest, Sierra Nevada, USA, Atmos. Chem. Phys. Discuss., 7, 14139–14169, 2007, http://www.atmos-chem-phys-discuss.net/7/14139/2007/.

Flocke, F., Volz-Thomas, A., Buers, H. J., Patz, W., Garthe, H. J., and Kley, D.: Long-term measurements of alkyl nitrates in southern Germany 1. General behavior and seasonal and diurnal variation, J. Geophys. Res., 103, 5729–5746, 1998.

Fountoukis, C., Nenes, A., Sullivan, A., Weber, R., VanReken, T., Fischer, M., Matas, E., Moya, M., Farmer, D., and Cohen, R. C.: Thermodynamic characterization of Mexico City aerosol during MILAGRO 2006, Atmos. Chem. Phys. Discuss., 7, 9203–9233, 2007, http://www.atmos-chem-phys-discuss.net/7/9203/2007/.

Fried, A., McKeen, S., Sewell, S., Harder, J., Henry, B., Goldan, P., Kuster, W., Williams, E., Baumann, K., Shetter, R., and Cantrell, C.: Photochemistry of formaldehyde during the 1993 Tropospheric OH Photochemistry Experiment, J. Geophys. Res., 102, 6283–6296, 1997.

Fuentes, J. D., Lerdau, M., Atkinson, R., Baldocchi, D., Bottenheim, J. W., Ciccioli, P., Lamb, B., Geron, C., Gu, L., Guenther, A., Sharkey, T. D., and Stockwell, W.: Biogenic hydrocarbons in the atmospheric boundary layer: A review, B. Am. Meteorol. Soc., 81, 1537–1575, 2000.

Giacopelli, P., Ford, K., Espada, C., and Shepson, P. B.: Comparison of the measured and simulated isoprene nitrate distributions above a forest canopy, J. Geophys. Res., 110, D01304, doi:10.1029/2004JD005123, 2005.

Goldstein, A. H., Hultman, N. E., Fracheboud, J. M., Bauer, M. R., Panek, J. A., Xu, M., Qi, Y., Guenther, A. B., and Baugh, W.: Effects of climate variability on the carbon dioxide, water, and sensible heat fluxes above a ponderosa pine plantation in the Sierra Nevada (CA), Agr. Forest Meteorol., 101, 113–129, 2000.

Goldstein, A. H. and Schade, G. W.: Quantifying biogenic and anthropogenic contributions to

acetone mixing ratios in a rural environment, Atmos. Environ., 34, 4997–5006, 2000.

Grossenbacher, J. W., Couch, T., Shepson, P. B., Thornberry, T., Witmer-Rich, M., Carroll, M. A., Faloona, I., Tan, D., Brune, W., Ostling, K., and Bertman, S.: Measurements of isoprene nitrates above a forest canopy, J. Geophys. Res., 106, 24429–24438, 2001.

Grossenbacher, J. W., Barket, D. J., Shepson, P. B., Carroll, M. A., Olszyna, K., and Apel, E.: A comparison of isoprene nitrate concentrations at two forest-impacted sites, J. Geophys. Res., 109, D11311, doi:10.1029/2003JD003966, 2004.

Hauglustaine, D. A., Madronich, S., Ridley, B. A., Walega, J. G., Cantrell, C. A., Shetter, R. E., and Hubler, G.: Observed and model-calculated photostationary state at Mauna Loa observatory during MLOPEX 2, J. Geophys. Res., 101, 14681–14696, 1996.

Herman, D. J., Halverson, L. J., and Firestone, M. K.: Nitrogen dynamics in an annual grassland: Oak canopy, climate, and microbial population effects, Ecol. Appl., 13, 593–604, 2003.

Holzinger, R., Lee, A., McKay, M., and Goldstein, A. H.: Seasonal variability of monoterpene emission factors for a ponderosa pine plantation in California, Atmos. Chem. Phys., 6, 1267–1274, 2006,
http://www.atmos-chem-phys.net/6/1267/2006/.

Horii, C. V.: Tropospheric reactive nitrogen speiciation, deposition, and chemistry at Harvard Forest, Ph.D. thesis, Department of Earth and Planetary Sciences, Harvard University, Cambridge, 148 pp., 2002.

Horowitz, L. W., Fiore, A. M., Milly, G. P., Cohen, R. C., Perring, A., Wooldridge, P. J., Hess, P. G., Emmons, L. K., and Lamarque, J.-F.: Observational constraints on the chemistry of isoprene over the eastern U.S., J. Geophys. Res., 112, D12S08, doi:10.1029/2006JD007747, 2007.

Kleinman, L., Lee, Y. N., Springston, S. R., Nunnermacker, L., Zhou, X. L., Brown, R., Hallock, K., Klotz, P., Leahy, D., Lee, J. H., and Newman, L.: Ozone formation at a rural site in the Southeastern United States, J. Geophys. Res., 99, 3469–3482, 1994.

Kroll, J. H., Ng, N. L., Murphy, S. M., Flagan, R. C., and Seinfeld, J. H.: Secondary organic aerosol formation from isoprene photooxidation, Environ. Sci. Technol., 40, 1869–1877, 2006.

Kurpius, M. R., McKay, M., and Goldstein, A. H.: Annual ozone deposition to a Sierra Nevada ponderosa pine plantation, Atmos. Environ., 36, 4503–4515, 2002.

Kurpius, M. R., Panek, J. A., Nikolov, N. T., McKay, M., and Goldstein, A. H.: Partitioning of water flux in a Sierra Nevada ponderosa pine plantation, Agr. Forest Meteorol., 117, 173–

192, 2003.

LaFranchi, B. W., Wolfe, G. M., Thornton, J. A., Browne, E. C., Min, K. E., Wooldridge, P. J., Cohen, R. C., McKay, M., Goldstein, A. H., Gilman, J. B., Welsh-Bon, D., Kuster, W. C., deGouw, J. A., Mao, J., Ren, X., Chen, Z., and Brune, W. H.: Closing the peroxy acetyl (PA) radical budget: observations of acyl peroxy nitrates (PAN, PPN, and MPAN) during BEARPEX 2007, Eos Trans. AGU, 89(53), Fall Meet. Suppl., San Francisco, USA, 15–19 December 2008, A41F-0188, 2008.

Lamanna, M. S. and Goldstein, A. H.: In situ measurements of C_2-C_{10} volatile organic compounds above a Sierra Nevada ponderosa pine plantation, J. Geophys. Res., 104, 21247–21262, 1999.

Lee, A., Schade, G. W., Holzinger, R., and Goldstein, A. H.: A comparison of new measurements of total monoterpene flux with improved measurements of speciated monoterpene flux, Atmos. Chem. Phys., 5, 505–513, 2005, http://www.atmos-chem-phys.net/5/505/2005/.

Lefer, B. L., Talbot, R. W., and Munger, J. W.: Nitric acid and ammonia at a rural northeastern U.S. site, J. Geophys. Res., 104, 1645–1661, 1999.

Mihele, C. M. and Hastie, D. R.: Radical chemistry at a forested continental site: Results from the PROPHET 1997 campaign, J. Geophys. Res., 108, 4450, doi:10.1029/2002JD002888, 2003.

Munger, J. W., Wofsy, S. C., Bakwin, P. S., Fan, S. M., Goulden, M. L., Daube, B. C., Goldstein, A. H., Moore, K. E., and Fitzjarrald, D. R.: Atmospheric deposition of reactive nitrogen oxides and ozone in a temperate deciduous forest and a subarctic woodland 1. Measurements and Mechanisms, J. Geophys. Res., 101, 12639–12657, 1996.

Munger, J. W., Fan, S. M., Bakwin, P. S., Goulden, M. L., Goldstein, A. H., Colman, A. S., and Wofsy, S. C.: Regional budgets for nitrogen oxides from continental sources: Variations of rates for oxidation and deposition with season and distance from source regions, J. Geophys. Res., 103, 8355–8368, 1998.

Murphy, J. G., Thornton, J. A., Wooldridge, P. J., Day, D. A., Rosen, R. S., Cantrell, C., Shetter, R. E., Lefer, B., and Cohen, R. C.: Measurements of the sum of HO_2NO_2 and $CH_3O_2NO_2$ in the remote troposphere, Atmos. Chem. Phys., 4, 377–384, 2004, http://www.atmos-chem-phys.net/4/377/2004/.

Murphy, J. G., Day, D. A., Cleary, P. A., Wooldridge, P. J., and Cohen, R. C.: Observations of the diurnal and seasonal trends in nitrogen oxides in the western Sierra Nevada, Atmos. Chem.

Phys., 6, 5321–5338, 2006,
http://www.atmos-chem-phys.net/6/5321/2006/.

Murphy, J. G., Day, D. A., Cleary, P. A., Wooldridge, P. J., Millet, D. B., Goldstein, A. H., and Cohen, R. C.: The weekend effect within and downwind of Sacramento – Part 1: Observations of ozone, nitrogen oxides, and VOC reactivity, Atmos. Chem. Phys., 7, 5327–5339, 2007, http://www.atmos-chem-phys.net/7/5327/2007/.

Neuman, J. A., Huey, L. G., Ryerson, T. B., and Fahey, D. W.: Study of inlet materials for sampling atmospheric nitric acid, Environ. Sci. Technol., 33, 1133–1136, 1999.

O'Brien, J. M., Shepson, P. B., Muthuramu, K., Hao, C., Niki, H., Hastie, D. R., Taylor, R., and Roussel, P. B.: Measurements of alkyl and multifunctional organic nitrates at a rural site in Ontario, J. Geophys. Res., 100, 22795–22804, 1995.

O'Brien, J. M., Shepson, P. B., Wu, Q., Biesenthal, T., Bottenheim, J. W., Wiebe, H. A., Anlauf, K. G., and Brickell, P.: Production and distribution of organic nitrates, and their relationship to carbonyl compounds in an urban environment, Atmos. Environ., 31, 2059–2069, 1997.

Ostling, K., Kelly, B., Bird, S., Bertman, S., Pippin, M., Thornberry, T., and Carroll, M. A.: Fast-turnaround alkyl nitrate measurements during the PROPHET 1998 summer intensive, J. Geophys. Res., 106, 24439–24449, 2001.

Parrish, D. D., Norton, R. B., Bollinger, M. J., Liu, S. C., Murphy, P. C., Albritoon, D. L., Fehsenfeld, F. C., and Heubert, B. J.: Measurements of HNO_3 and NO_3 particulates at a rural site in the Colorado mountains, J. Geophys. Res., 91, 5379–5393, 1986.

Parrish, D. D., Buhr, M. P., Trainer, M., Norton, R. B., Shimshock, J. P., Fehsenfeld, F. C., Anlauf, K. G., Bottenheim, J. W., Tang, Y. Z., Wiebe, H. A., Roberts, J. M., Tanner, R. L., Newman, L., Bowersox, V. C., Olszyna, K. J., Bailey, E. M., Rodgers, M. O., Wang, T., Berresheim, H., Roychowdhury, U. K., and Demerjian, K. L.: The total reactive oxidized nitrogen levels and the partitioning between the individual species at six rural sites in eastern North America, J. Geophys. Res., 98, 2927–2939, 1993.

Patchen, A. K., Pennino, M. J., Kiep, A. C., and Elrod, M. J.: Direct kinetics study of the product-forming channels of the reaction of isoprene-derived hydroxyperoxy radicals with NO, Int. J. Chem. Kinet., 39, 353–361, doi:10.1002/kin.20248, 2007.

Paulot, F., D. Crounse, J., Kjaergaard, H. G., Kroll, J. H., Seinfeld, J. H., and Wennberg, P. O.: Isoprene photooxidation mechanism: resonance channels and implications for the production of nitrates and acids, Atmos. Chem. Phys. Discuss., 8, 14643–14716, 2008, http://www.atmos-chem-phys-discuss.net/8/14643/2008/.

Title Page

Abstract	Introduction
Conclusions	References
Tables	Figures

◄ | ►

◄ | ►

Back | Close

Full Screen / Esc

Printer-friendly Version

Interactive Discussion

Pérez, I. M., Wooldridge, P. J., and Cohen, R. C.: Laboratory evaluation of a novel thermal dissociation chemiluminescence method for in situ detection of nitrous acid, Atmos. Environ., 41, 3993–4001, 2007.

Pérez, I. M.: The photochemical evolution of the Sacramento urban plume: A guide to controlling ozone now and in a warmer climate, Ph.D. thesis, Department of Chemistry, University of California, Berkeley, 2008.

Pérez, I. M. and Cohen, R. C.: A Lagrangian model of the chemical composition of an urban plume 1: nitrogen oxides, in preparation, 2009.

Perring, A. E., Bertram, T. H., Wooldridge, P. J., Fried, A., Heikes, B. G., Dibb, J., Crounse, J. D., Wennberg, P. O., Blake, N. J., Brune, W. H., Blake, D. R., and Cohen, R. C.: Airborne observations of total $RONO_2$: new constraints on the yield and lifetime of isoprene nitrates, Atmos. Chem. Phys. Discuss., 8, 12313–12341, 2008, http://www.atmos-chem-phys-discuss.net/8/12313/2008/.

Roberts, J. M., Tanner, R. L., Newman, L., Bowersox, V. C., Bottenheim, J. W., Anlauf, K. G., Brice, K. A., Parrish, D. D., Fehsenfeld, F. C., Buhr, M. P., Meagher, J. F., and Bailey, E. M.: Relationships between pan and ozone at sites in eastern North America, J. Geophys. Res., 100, 22821–22830, 1995.

Roberts, J. M., Stroud, C. A., Jobson, B. T., Trainer, M., Hereid, D., Williams, E., Fehsenfeld, F., Brune, W., Martinez, M., and Harder, H.: Application of a sequential reaction model to PANs and aldehyde measurements in two urban areas, Geophys. Res. Lett., 28, 4583–4586, 2001.

Romero, M. T. B., Blitz, M. A., Heard, D. E., Pilling, M. J., Price, B., Seakins, P. W., and Wang, L. M.: Photolysis of methylethyl, diethyl and methylvinyl ketones and their role in the atmospheric HOx budget, Faraday Discuss., 130, 73–88, doi:10.1039/b419160a, 2005.

Rosen, R. S., Wood, E. C., Wooldridge, P. J., Thornton, J. A., Cohen, R. C., Williams, E. J., Roberts, J. M., Jobson, T. B., and Kuster, W.: Observations of total alkyl nitrates during TEXAQS-2000, AGU Fall Meeting, San Francisco, USA, 6–10 December 2002, Conference Poster, 2002.

Rosen, R. S., Wood, E., Wooldridge, P. J., Thornton, J. A., Day, D. A., Kuster, B., Williams, E. J., Jobson, B. T., and Cohen, R. C.: Observations of total alkyl nitrates during Texas Air Quality Study 2000: Implications for O_3 and alkyl nitrate photochemistry, J. Geophys. Res., 107, D07303, doi:07310.01029/02003JD004227, 2004.

Ryerson, T. B., Huey, L. G., Knapp, K., Neuman, J. A., Parrish, D. D., Sueper, D. T., and Fehsen-

feld, F. C.: Design and initial characterization of an inlet for gas-phase NO_y measurements from aircraft, J. Geophys. Res., 104, 5483–5492, 1999.

Sander, S. P., Friedl, R. R., Ravishankara, A. R., Golden, D. M., Kolb, C. E., Kurylo, M. J., Molina, M. J., Moortgat, G. K., Heller-Rudek, H., Finlayson-Pitts, B. J., Wine, P. H., Huie, R. E., and Orkin, V. L.: Chemical kinetics and photochemical data for use in atmospheric studies, Evaluation Number 15, National Aeronautics and Space Administration; Jet Propulsion Laboratory California Institute of Technology, Pasadena, California, 523 pp., 2006.

Schade, G. W. and Crutzen, P. J.: CO emissions from degrading plant matter (II). Estimate of a global source strength, Tellus B, Chem. Phys. Meteorol., 51, 909–918, 1999.

Schade, G. W., Goldstein, A. H., and Lamanna, M. S.: Are monoterpene emissions influenced by humidity?, Geophys. Res. Lett., 26, 2187–2190, 1999a.

Schade, G. W., Hofmann, R. M., and Crutzen, P. J.: CO emissions from degrading plant matter (I). Measurements, Tellus B, Chem. Phys. Meteorol., 51, 889–908, 1999b.

Schade, G. W. and Goldstein, A. H.: Fluxes of oxygenated volatile organic compounds from a ponderosa pine plantation, J. Geophys. Res., 106, 3111–3123, 2001.

Schneider, M., Luxenhofer, O., Deissler, A., and Ballschmiter, K.: C-1-C-15 alkyl nitrates, benzyl nitrate, and bifunctional nitrates: Measurements in California and South Atlantic air and global comparison using C2Cl4 and CHBr3 as marker molecules, Environ. Sci. Technol., 32, 3055–3062, 1998.

Seaman, N. L., Stauffer, D. R., and Lariogibbs, A. M.: A multiscale four-dimensional data assimilation system applied in the San Joaquin Valley during SARMAP .1. Modeling design and basic performance characteristics, J. Appl. Meteorol., 34, 1739–1761, 1995.

Shepson, P. B., Hastie, D. T., So, K. W., and Schiff, H. I.: Relationship between PAN, PPN, and O_3 at urban and rural sites in Ontario, Atmos. Environ., 26A, 1259–1270, 1992.

Singh, H. B., Herlth, D., Ohara, D., Zahnle, K., Bradshaw, J. D., Sandholm, S. T., Talbot, R., Crutzen, P. J., and Kanakidou, M.: Relationship of peroxyacetyl nitrate to active and total odd nitrogen at northern high latitudes: Influence of reservoir species on No_x and O_3, J. Geophys. Res., 97, 16523–16530, 1992.

Smyth, S. B., Sandholm, S. T., Bradshaw, J. D., Talbot, R. W., Blake, D. R., Blake, N. J., Rowland, F. S., Singh, H. B., Gregory, G. L., Anderson, B. E., Sachse, G. W., Collins, J. E., and Bachmeier, A. S.: Factors influencing the upper free tropospheric distribution of reactive nitrogen over the South Atlantic during the TRACE A experiment, J. Geophys. Res.-Atmos., 101, 24165–24186, 1996.

Title Page

Abstract | Introduction

Conclusions | References

Tables | Figures

◄◄ | ►►

◄ | ►

Back | Close

Full Screen / Esc

Printer-friendly Version

Interactive Discussion

Spaulding, R. S., Schade, G. W., Goldstein, A. H., and Charles, M. J.: Characterization of secondary atmospheric photooxidation products: Evidence for biogenic and anthropogenic sources, J. Geophys. Res., 108, 4247, doi:10.1029/2002JD002478, 2003.

Sprengnether, M., Demerjian, K. L., Donahue, N. M., and Anderson, J. G.: Product analysis of the OH oxidation of isoprene and 1,3-butadiene in the presence of NO, J. Geophys. Res., 107, 4268, doi:10.1029/2001JD000716, 2002.

Thornberry, T., Carroll, M. A., Keeler, G. J., Sillman, S., Bertman, S. B., Pippin, M. R., Ostling, K., Grossenbacher, J. W., Shepson, P. B., Cooper, O. R., Moody, J. L., and Stockwell, W. R.: Observations of reactive oxidized nitrogen and speciation of NO_y during the PROPHET summer 1998 intensive, J. Geophys. Res., 106, 24359–24386, 2001.

Thornton, J. A., Wooldridge, P. J., and Cohen, R. C.: Atmospheric NO_2: In situ laser-induced fluorescence detection at parts per trillion mixing ratios, Anal. Chem., 72, 528–539, 2000.

Thornton, J. A., Wooldridge, P. J., Cohen, R. C., Martinez, M., Harder, H., Brune, W. H., Williams, E. J., Fehsenfeld, F. C., Hall, S. R., Shetter, R. E., Wert, B. P., and Fried, A.: Observations of ozone production rates as a function of NO_2 abundances and HO_x production rates in the Nashville urban plume, J. Geophys. Res., 107, 4146, doi:10.1029/2001JD000932, 2002.

Trainer, M., Buhr, M. P., Curran, C. M., Fehsenfeld, F. C., Hsie, E. Y., Liu, S. C., Norton, R. B., Parrish, D. D., Williams, E. J., Gandrud, B. W., Ridley, B. A., Shetter, J. D., Allwine, E. J., and Westberg, H. H.: Observations and modeling of the reactive nitrogen photochemistry at a rural site, J. Geophys. Res., 96, 3045–3063, 1991.

Tuazon, E. C. and Atkinson, R.: A product study of the gas-phase reaction of isoprene with the OH radical in the presence of NO_x, Int. J. Chem. Kinet., 22, 1221–1236, 1990.

UCAR/NCAR/ACD: Tropospheric Ultraviolet and Visible (TUV) Radiation Model: http://cprm.acd.ucar.edu/Models/TUV/, 2006.

Wildt, J., Kley, D., Rockel, A., Rockel, P., and Segschneider, H. J.: Emission of NO from several higher plant species, J. Geophys. Res., 102, 5919–5927, 1997.

Woidich, S., Froescheis, O., Luxenhofer, O., and Ballschmiter, K.: EI- and NCI-mass spectrometry of arylalkyl nitrates and their occurrence in urban air, Fresen. J. Anal. Chem., 364, 91–99, 1999.

Zellweger, C., Ammann, M., Buchmann, B., Hofer, P., Lugauer, M., Ruttimann, R., Streit, N., Weingartner, E., and Baltensperger, U.: Summertime NO_y speciation at the Jungfraujoch, 3580 m above sea level, Switzerland, J. Geophys. Res., 105, 6655–6667, 2000.

Title Page

Abstract | Introduction

Conclusions | References

Tables | Figures

◄ | ►

◄ | ►

Back | Close

Full Screen / Esc

Printer-friendly Version

Interactive Discussion

Table 1. Number of 30-min points used and percent of coverage for dataset.

Compound	No. of 30-min Points	% Coverage[a]
NO (chemiluminescence)	2943 (7965)	50.3, (25.5)
NO (chemi.+estimated)[b]	4475 (15098)	76.4, (48.4)
NO_2	3664 (11595)	62.6, (37.2)
ΣPNs	3517 (10877)	60.1, (34.9)
ΣANs	3564 (10936)	60.9, (35.1)
HNO_3	3635 (10608)	62.1, (34.0)
ΣNO_{yi}	3508 (10195)	59.9, (32.7)
CO	4536 (18448)	77.5, (59.1)
O_3	5566 (29146)	95.0, (93.4)

[a] Percent coverage of the summer period from 1 June through 30 September 2001 and for all data 3 October 2000–9 February 2002 (in parenthesis).
[b] Data acquired directly with chemiluminescence instrument in addition to estimates of NO based on NO_2 and O_3 measurements.
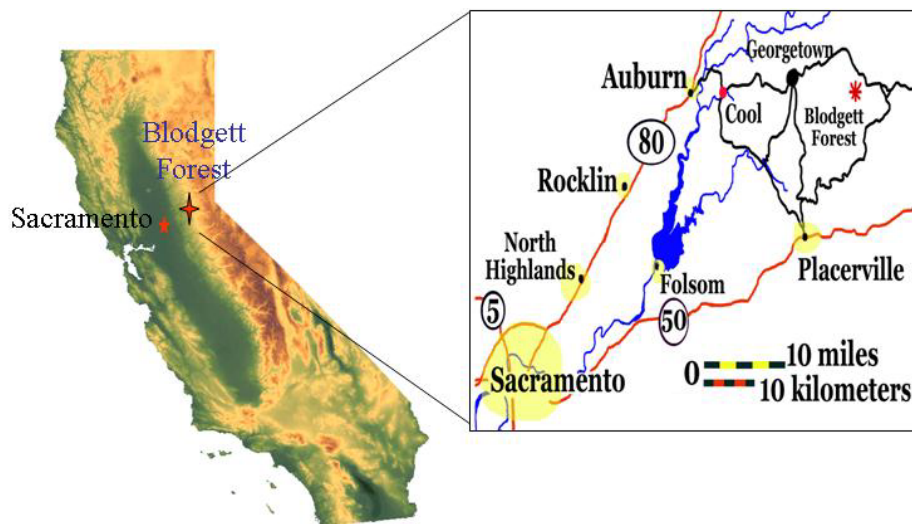
Fig. 1. Relief map of California showing blow-up of Sacramento to Blodgett Forest region.
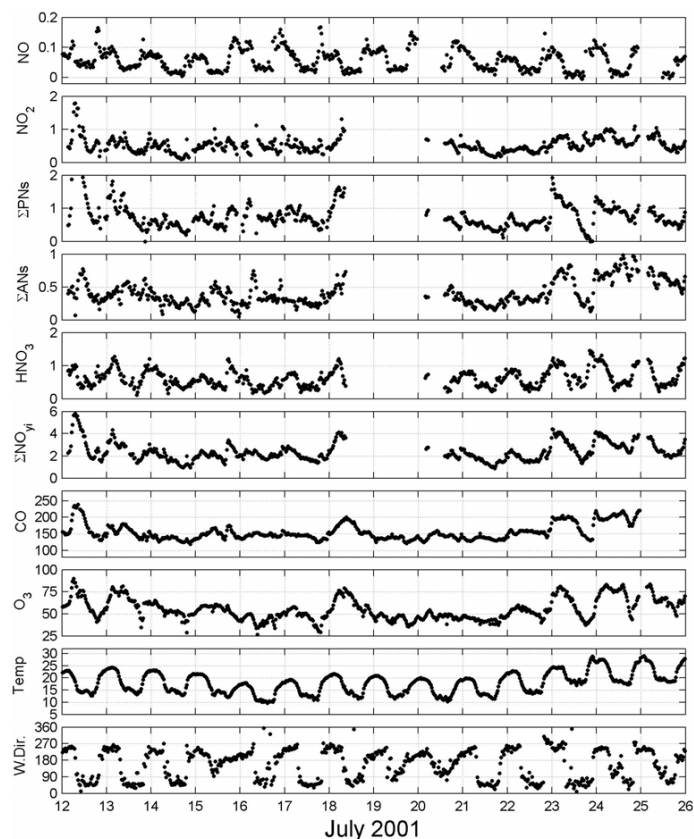
Fig. 2a. Observations of NO, NO_2, ΣPNs, ΣANs, HNO_3, $ΣNO_{yi}$, CO, O_3, temperature (°C), and wind direction for **(a)** July 2001, **(b)** June 2001, and **(c)** September 2001. Data are 30-min medians except ozone and wind direction which are 30-min means. All concentrations are in ppb.

Fig. 2b. Continued.

Fig. 2c. Continued.

Fig. 3. ΣNO_{yi}, CO, O_3, temperature (˚C) and wind direction for summer 2001 (weekdays only). Data are 30-min medians and lines bound the central 68th percentile. All concentrations are in ppb.
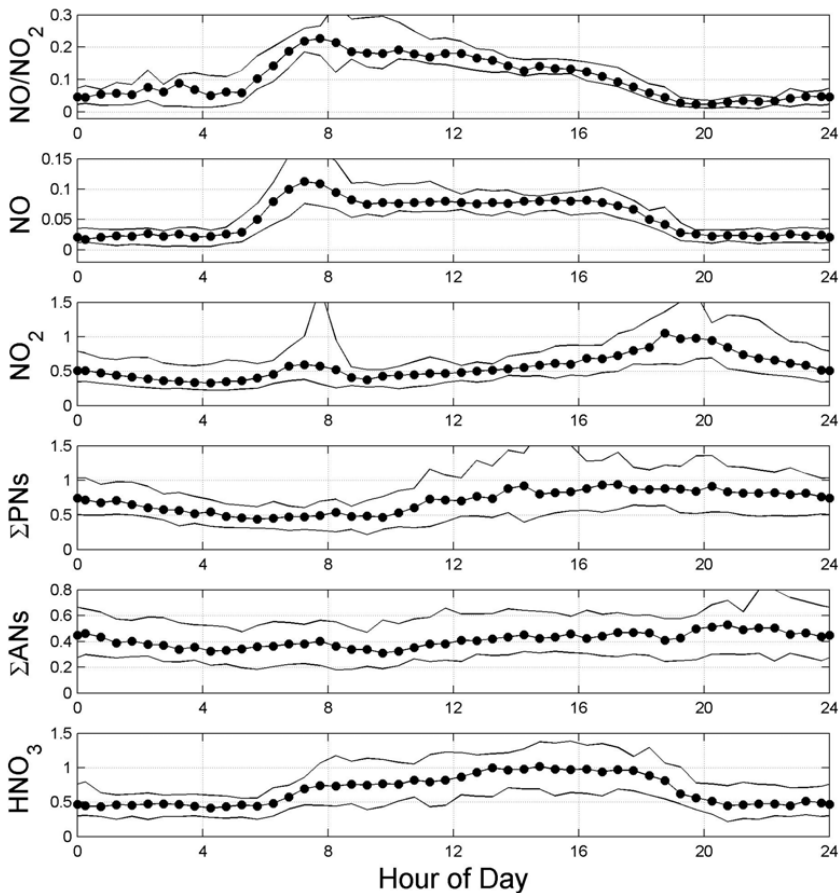
Fig. 4. NO/NO$_2$, NO, NO$_2$, ΣPNs, ΣANs and HNO$_3$ for summer 2001 (weekdays only). Data are 30-min medians and lines bound the central 68th percentile. All concentrations are in ppb.
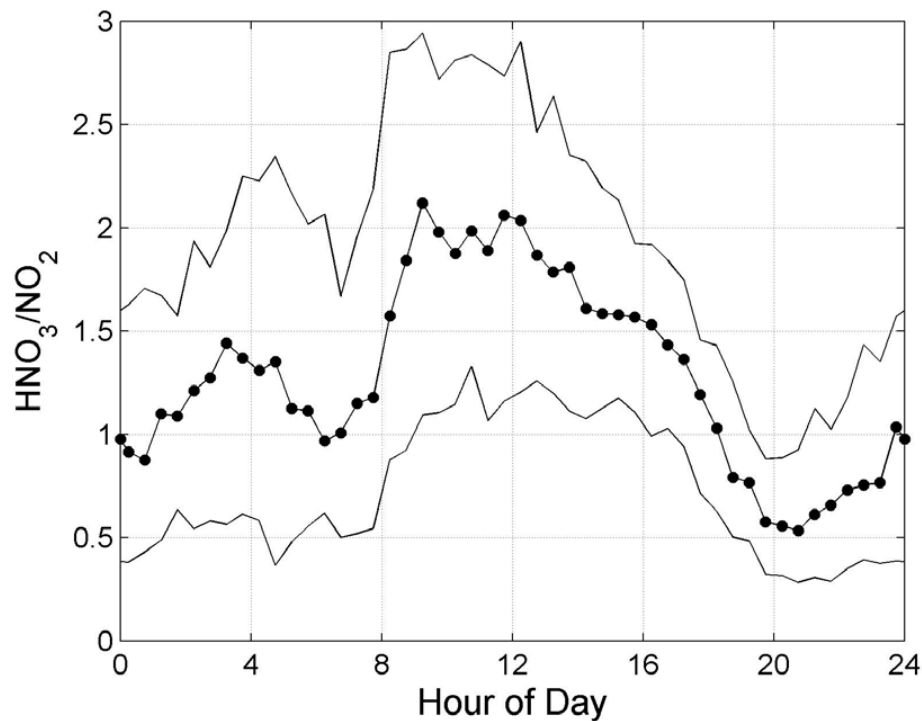
Fig. 5. HNO_3/NO_2 for summer 2001 (weekdays only). Data are 30-min medians and lines bound the central 68th percentile.
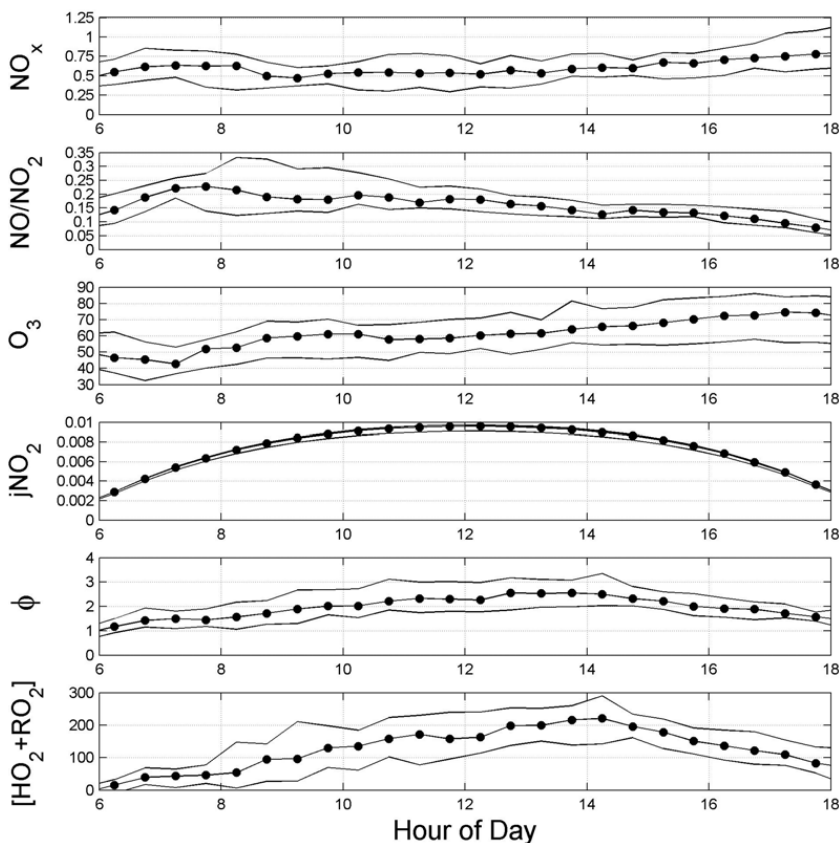
Fig. 6. NO_x, NO/NO_2, O_3, ϕ, and modeled [HO_2+RO_2] during daytime for summer 2001 (weekdays only). Averages are from only when measurements of NO, NO_2, and O_3 where all available. Data are 30-min medians and lines bound the central 68th percentile. All concentrations are in ppb except [HO_2+RO_2] is ppt.